NAVAL POSTGRADUATE SCHOOL
Monterey, California

THESIS

Elevated Temperature properties of a Dispersion Strengthened Al-[Fe, V, Si] Alloy

by

Matthew B. Cissel

December, 1991

Thesis Advisor: Shantanu Mitra

UNCLASSIFIED
SECURITY CLASSIFICATION OF THIS PAGE

REPORT DOCUMENTATION PAGE

Form Approved
OMB No. 0704-0188

1a REPORT SECURITY CLASSIFICATION UNCLASSIFIED	1b RESTRICTIVE MARKINGS
2a SECURITY CLASSIFICATION AUTHORITY	3 DISTRIBUTION / AVAILABILITY OF REPORT Approved for public release
2b DECLASSIFICATION / DOWNGRADING SCHEDULE	distribution is unlimited
4 PERFORMING ORGANIZATION REPORT NUMBER(S)	5 MONITORING ORGANIZATION REPORT NUMBER(S)
6a NAME OF PERFORMING ORGANIZATION Naval Postgraduate School 6b OFFICE SYMBOL (If applicable)	7a NAME OF MONITORING ORGANIZATION Naval Postgraduate School
6c ADDRESS (City, State, and ZIP Code) Monterey, California 93943-5000	7b ADDRESS (City, State, and ZIP Code) Monterey, California 93943-500
8a NAME OF FUNDING / SPONSORING ORGANIZATION 8b OFFICE SYMBOL (If applicable)	9 PROCUREMENT INSTRUMENT IDENTIFICATION NUMBER
8c ADDRESS (City, State, and ZIP Code)	10 SOURCE OF FUNDING NUMBERS PROGRAM ELEMENT NO / PROJECT NO / TASK NO / WORK UNIT ACCESSION NO

11 TITLE (Include Security Classification)

Elevated Temperature Properties of a Dispersion Strengthened Al-(Fe, V, Si) Alloy

12 PERSONAL AUTHOR(S)
Matthew B. Cissel

13a TYPE OF REPORT	13b TIME COVERED	14 DATE OF REPORT (Year, Month, Day)	15 PAGE COUNT
Thesis, M.S.	FROM _____ TO _____	December 1991	72

16 SUPPLEMENTARY NOTATION The views expressed in this thesis are those of the author and do not reflect the official policy or position of the Department of Defense or U.S. Government.

17 COSATI CODES			18 SUBJECT TERMS (Continue on reverse if necessary and identify by block number)
FIELD	GROUP	SUB-GROUP	Dispersion Strengthened Al-Fe-V-Si Alloy

19 ABSTRACT (Continue on reverse if necessary and identify by block number)

The mechanical properties at elevated temperatures of a new dispersion strengthened Al-Fe-V-Si (FVS1212) alloy were evaluated. Constant extension rate (tension) tests were conducted on an Instron machine and strain rate sensitivity, yield stress and elongation changes with temperature were obtained. The mechanical behavior appeared to change at approximately 250°C, with intergranular fracture and necking occurring at low temperatures; and transgranular dimples with uniform plastic deformatiom at high temperatures. Creep tests in tension were conducted and the stress dependence n, of the steady state creep rate was obtained. Achange in the n value was seen from 16 down to 4 at low stresses and temperatures. The activation energy for creepwas calculated from the slope of steady state creep rate vs 1/temperature plot and from an iterative technique based on plotting all the data on one curve using an approximate value of activation energy for the temperature compensated strain rate plotted against the modulus compensated stress.

(continued on back)

20 DISTRIBUTION / AVAILABILITY OF ABSTRACT	21 ABSTRACT SECURITY CLASSIFICATION	
☒ UNCLASSIFIED/UNLIMITED ☐ SAME AS RPT ☐ DTIC USERS	UNCLASSIFIED	
22a NAME OF RESPONSIBLE INDIVIDUAL Adjunct Professor Shantanu Mitra	22b TELEPHONE (Include Area Code) 408-646-2551	22c OFFICE SYMBOL ME/MT

DD Form 1473, JUN 86 *Previous editions are obsolete.* SECURITY CLASSIFICATION OF THIS PAGE

S/N 0102-LF-014-6603 UNCLASSIFIED

The first technique gave values between 100kJ/mole - 1000 kJ/mole, while the second method yielded 400 (± 20) kJ/mole. The creep behavior of this alloy appeared to exhibit a threshold stress of 7×10^{-4}E.

Approved for public release; distribution is unlimited.

Elevated Temperature Properties of a Dispersion Strengthened Al-[Fe, V, Si] Alloy

by

Matthew B. Cissel
Lieutenant, United States Navy
B.S., United States. Naval Academy, 1982

Submitted in partial fulfillment
of the requirements for the degree of

MASTER OF SCIENCE IN ENGINEERING SCIENCE

from the

NAVAL POSTGRADUATE SCHOOL
December 1991

Author: Matthew B Cissel
Matthew B. Cissel

Approved by: Shantanu Mitra
Shantanu Mitra, Thesis Advisor

Terry R. McNelley, Second Reader

A. J. Healey, Chairman
Department of Mechanical Engineering

ABSTRACT

The mechanical properties at elevated temperatures of a new dispersion strengthened Al-Fe-V-Si (FVS1212) alloy were evaluated. Constant extension rate (tension) tests were conducted on an Instron machine and strain rate sensitivity, yield strength and elongation changes with temperature were obtained. The mechanical behavior appeared to change at ≈ 250°C, with intergranular fracture and necking occurring at low temperatures; and transgranular dimples with uniform plastic deformation at high temperatures. Creep tests in tension were conducted and the stress dependence n, of the steady state creep rate was obtained. A change in the n value was seen from 16 down to 4 at low stresses and temperatures. The activation energy for creep was calculated from the slope of steady state creep rate vs. 1/Temperature (1/T) plot and from an iterative technique based on plotting all the data on one curve using an appropriate value of activation energy for the temperature compensated strain rate plotted against the modulus compensated stress. The first technique gave values between 100 kJ/mole - 1000 kJ/mole, while the second method yielded 400 (± 20) kJ/mole. The creep behavior of this alloy appeared to exhibit a threshold stress of $7 \times 10^{-4}E$.

TABLE OF CONTENTS

LIST OF FIGURES

I. INTRODUCTION

Attempts to improve the elevated temperature properties of aluminum based alloys dates back to the late 1940's, when an oxide dispersion strengthened aluminum was developed [ref 1]. The pioneering work on sintered aluminum products (SAP) led to the development of other types of dispersion strengthened aluminum alloys. With the introduction of gas atomization techniques, researchers were able to further explore the formation of aluminum based alloys containing relatively high non-equilibrium levels of solute elements and powder metallurgy routes to fabricate particulate composites (reinforced with hard ceramics). The rapid solidification process (RSP), based on cooling rates $\approx 10^{-7}$ K/sec, developed later, has benefits that include increased solid solubility limits, fine-scale microstructure and compositional homogeneity. Precipitation of hard intermetallic dispersoids from the matrix was then controlled to achieve some strengthening effects via dispersion hardening. The ability to achieve a fine uniform dispersion of an insoluble constituent in an aluminum matrix created alloys that exhibited superior mechanical properties, such as high strength and stiffness, elevated temperature performance coupled with excellent corrosion and wear resistance. A new class of dispersion strengthened aluminum alloys, based on the

RSP technique, involves precipitation of an intermetallic dispersoid during the rapid solidification process itself. This class of alloy continues to demonstrate excellent potential especially in the aerospace industry. These dispersion strengthened alloys are based on the Al-Fe, V, Si system and comprise $Al_{12}(Fe, V)_3Si$ intermetallic dispersoids in an Al matrix that has Fe, V and Si in solid solution. There are still several barriers which continue to limit their application and complete acceptance. Some of these barriers include cost especially due to the production route needed to rapidly solidify the thin ribbons and then powder compact to obtain larger sizes. These alloys typically have large volume fraction of dispersoids ($\approx$ 40%) and are believed to have increased coherence at the dispersoid/matrix interfaces. A comprehensive study of the elevated temperature mechanical properties of this alloy system is lacking and forms the basis of this study.

II. BACKGROUND

A. EARLY DEVELOPMENT OF ALUMINUM ALLOYS FOR ELEVATED TEMPERATURES.

The initial success in manufacturing elevated temperature aluminum alloys came through the dispersion of fine Al_2O_3 scales which were incorporated into a compact made from powdered aluminum, called sintered aluminum products (SAP). With the development of SAP type alloys, researchers continued to look for ways to further improve the properties of aluminum alloys, especially the high temperature ones. The next generation of aluminum alloys appeared with the introduction of atomization. This enabled rapid cooling rates and saturation of solute elements in the aluminum matrix that could be later precipitated out. More importantly, the aluminum powder could be mixed with a number of dispersoid particulates to form particulate composites. Atomization thus laid the ground work for the development of the current aluminum powder metallurgy (PM) alloys.

The current generation of aluminum alloys under study here utilizes the rapid solidification process to disperse a very fine intermetallic dispersoid in an aluminum matrix during the solidification process itself [ref 1]. Another family of aluminum alloys, potentially for high temperature

applications, is also based on non-equilibrium solutions and utilizes mechanical alloying techniques. They are based on processes such as ball milling and have met with partial success to date.

B. ALUMINUM ALLOYS THROUGH RAPID SOLIDIFICATION PROCESSING (RSP)

The ability to supersaturate an aluminum matrix with solute elements and to control the final microstructure through the formation in situ of fine dispersoid reinforcements (< 0.5 microns) has created great potential for various aluminum alloys. The RSP process enabled researchers to disperse from 5% to 40% volume fraction of insoluble intermetallic aluminide phases into an aluminum matrix [ref 1]. The fine dispersoids are normally less than 0.5 micron and are formed during the atomization of the alloy melt. There are various RSP techniques in use today, and melt spinning/planar flow casting (Figure 1) has been successful in producing a uniformly dispersed microstructure throughout the whole thickness of the as cast ribbon [ref 2]. These dispersoids are formed during the atomization process itself, and the high cooling rates (approximately 10^8 K/sec) [ref 1] ensure the fineness of the microstructure by increasing nucleation rates and limiting coarsening. The aspect of reproducibility and the uniformly dispersed microstructure is

very crucial during the processing if an aluminum alloy is to maintain its high temperature properties.

One of the first dispersion strengthened aluminum alloys systems where the RSP technique was used is the Al-Fe binary system. It was found that binary Al-Fe alloys containing between 7.5 wt% and 13 wt% Fe exhibited greatly improved tensile strength at high temperatures (up to 425°C) [ref 1]. The high temperature strength was attributed to the thermodynamic stability and resistance to coarsening of the dispersed aluminides. In studying the microstructure of these alloys after being rapidly solidified it was found that two distinct zones were present, designated as zone A and zone B. Zone A appeared optically featureless up to 1000x at which magnification a very fine dendritic or micro-cellular structure was noted. Zone B consisted of a much coarser structure and was formed on the air-side of the melt spin ribbon. Microhardness tests showed that zone A was approximately twice as hard as zone B, with no significant changes up to 200°C [ref 1]. Figure 2 shows a typical microstructure of the RSP Al-Fe system, taken from [ref 2], showing both zones. It was also found that through the proper control of the melt spinning/planar flow casting technique the material had a uniform zone A microstructure, and the zone B microstructure was suppressed [ref 3].

Cotton and Kaufman [ref 4] have proposed a mechanism for the development of the microstructure of the RSP Al-Fe based

alloys. The dispersed intermetallic phases are thought to form as primary phases during solidification, followed by planar, micro-cellular or cellular growth of the aluminum matrix. This mechanism can explain the random orientation, small size and intercellular location of the dispersoids.

Further research found that increased improvement in the high temperature properties could be obtained in Al-Fe alloys by the addition of other elements. This introduced ternary and quaternary addition to the Al-Fe alloys. Some examples of the more promising ones are Al-Fe-Si, Al-Fe-V, Al-Fe-Ce and Al-Fe-Mo. A microstructural study of the RSP Al-Fe-Si alloy identified $Al_{12}Fe_3Si$ as the intermetallic dispersoid in the cast ribbon that was produced upon melt spinning. It was found [ref 5] that this dispersoid was metastable and upon further working of the alloy such as by hot extrusion, the $Al_{12}Fe_3Si$ dispersoid transformed into a stable Al_3Fe_4 and Al_8Fe_2Si. These two stable dispersoids also coarsened during the process of hot working causing the alloy to lose most of its high temperature properties.

The next development in the Al-Fe-Si alloy system came with the discovery that the addition of vanadium to the alloy produced a stable $Al_{12}(Fe,V)_3Si$ intermetallic dispersoid [ref 6]. This dispersoid did not show any tendency to transform or coarsen upon further working of the alloy. The $Al_{12}(Fe,V)_3Si$ intermetallic has a complex body-centered cubic structure (Im3, with 138 atoms per unit cell) [ref 7]. It shows only

minimal coarsening at temperatures up to 500°C for 100 hours [ref 8], and it appears that the improved coherency between the dispersoid and the matrix may be responsible for the lack of driving force for the coarsening reaction.

C. MECHANICAL BEHAVIOR AND PROPERTIES OF Al-Fe-V-Si.

Alloys developed by Allied Signal Inc., Morristown, N.J., from the Al-Fe-V-Si system include FVS0611 (Al-6.5Fe-0.6V-1.3Si), FVS0812 (Al-8.5Fe-1.3V-1.7Si) and FVS1212 (Al-11.7Fe-1.3V-1.7Si). The effect of strain rate on the yield stress of alloy FVS0812 at temperatures ranging from 24°C to 321°C is shown in Figure 3. This plot shows a plateau in the yield stress, which appears to shift with a change in strain rate of the test. The plateau suggests some type of strengthening mechanism at that temperature range. Plateaus in yield stress vs. temperature plots have been well documented in pure aluminum, where they normally occur at room temperature.

The strengthening mechanism that has been associated with this phenomenon is dynamic strain aging (DSA) [ref 9, 10]. DSA involves the strengthening of the alloy during a test and is attributed to the interaction of a solute atmosphere with mobile dislocations [ref 9, 10]. Normally, mobile dislocation motion is too rapid for solute atoms to keep pace within the temperature region of DSA. However, models based on the dislocation arrest theory have concluded that solute atmospheres are formed around mobile dislocations when they

interact with forest dislocations that impede their motion. The effect is to enhance the strength of the material over the range of DSA. It also has an effect on the strain hardening rate which leads to localized plastic instability, neck formation, and a reduction in ductility [ref 9, 10]. The effect on strain rate sensitivity and elongation is evident in Figure 4 and Figure 5 respectively. Figure 4 shows a decrease in strain rate sensitivity for FVS0611 and FVS0812. This decrease is in the area where the plateau was found for the alloy FVS0812. Figure 5 shows a decrease in elongation in the same regions where the plateau was found in FVS0812 tested at strain rates of 8.89×10^{-5} sec^{-1} and 8.89×10^{-3} sec^{-1}. It has been shown [ref 11] that DSA is also associated with serrated plastic flow or jerky flow, also called the Portevin-Le Châtelier effect. In the Al-Si binary alloy this occurs around room temperature [ref 11] and it has been concluded that the diffusivity of Si in the aluminum matrix along with the silicon solute atom dislocation interaction is responsible for DSA. Bouchard et al [ref 11] have hypothesized that the occurrence of a plateau in the yield stress vs. temperature plot between 75 - 150°C, which coincided with a drop in the strain rate sensitivity, is due the presence of iron in the matrix. The higher activation energy for diffusion of iron (compare to silicon) led to a higher temperature range where DSA occurred compared with the effect of Si. Earlier it had been shown by Skinner et al [ref 9] that a ductility trough

existed in the FVS0611 alloy which was at lower temperatures than the ductility trough exhibited by FVS0812 in spite of the similar alloying elements. This can be attributed to the higher amounts of alloying elements in FVS0812 either through different matrix composition or, more probably through different volume fraction of dispersoids. No published data exist that addresses this point uniquely.

A detailed study of the mechanical behavior, as a function of temperature of FVS1212, an alloy with higher amounts of alloying element than FVS0812, at low strain rates, has not been reported to date. This investigation was thus undertaken to study the tensile behavior of FVS1212 at strain rates between 6.56×10^{-6} sec^{-1} and 6.56×10^{-5} sec^{-1} with temperatures ranging from room temperature up to 400°C.

D. CREEP BEHAVIOR OF DISPERSION STRENGTHENED ALLOYS.

Theoretical models for creep of particle hardened alloys given by Ansell and Weertman [ref 12] assume that dislocations were either bowing around or climbing over the particles. With this approach, it was shown that creep in particle strengthened alloy was similar to pure metals and most single phase alloys with respect to the stress dependence of the steady state creep rate. The stress exponent n, is defined as obtained from the power law of creep, which is given by

$$n = \frac{\partial \log \dot{\varepsilon}}{\partial \log \sigma} \Big|_{\varepsilon, T} \qquad (1)$$

Where $\dot{\epsilon}$ is the strain rate and σ is the stress. A constant value of n in the experimental data indicates power law creep and this is often described by

$$\dot{\epsilon}_s = B' \sigma^n \exp\left(-\frac{Q_c}{RT}\right) \qquad (2)$$

Where B' is a constant and Q_c is the activation energy for the creep process. In this form, the temperature dependence of creep is incorporated.

The stress exponent n was shown to be about 4 at high levels of stress and dropping to 1 at low stresses in the Ansell-Weertman model. However, it was experimentally found that in particle strengthened alloys the stress exponent and the activation energy for creep Q_c were much higher than expected. For example, in SAP, n was found to be $\approx$ 10 and Q_c ranged from 625 to 1675 kJ/mole. In pure aluminum n $\approx$ 5 and Q_c = 142 kJ/mole. In thoria dispersed (TD) nickel, which contains a small volume fraction of thoria particles dispersed in a nickel matrix, n values as high as 40 and $Q_c \approx$ 795 kJ/mole were found; whereas in unreinforced nickel, n = 5 and Q_c = 276 Kj/mole [ref 12].

Experimental results from copper-cobalt, where cobalt exists as a fine dispersoid in a copper matrix, are shown in Figure 6. Here the magnitude of the stress exponent decreases

with decreasing stress (i.e., n decreases from 12 to 5). Also if tangents are drawn from the n = 12 and n = 5 regions they intersect at a stress value which appears to be approximately equal to the yield stress of the material determined at rapid strain rates [ref 12]. Similar conclusions concerning other two phase alloys suggest that the high values of n and Q_c observed, occur at stresses exceeding the macroscopic yield stress [ref 12]. Surface examination of copper-cobalt alloy after creep has shown that slip bands are produced at high stress levels. The formation of these bands indicates that at stresses above macroscopic yield stress, the dislocations can either cut through or bow between particles. Whether a dislocation cuts through or bows between particles depends on the volume fraction, type and distribution of the particles present [ref 12]. Testing of TD-nichrome achieved some rather interesting results [ref 12], as shown in Figure 7 where $\dot{\epsilon}_s/D$ is plotted vs. σ/E. The conclusions made from these results are as follows;

1) At high stresses, the single crystal approaches the stress/creep rate relationship of polycrystalline nichrome. As stress decreases towards the calculated Orowan stress for bowing of dislocations between the ThO_2 dispersoids, the creep rate of TD-nichrome single crystal approaches zero.

2) Current theories predict creep to occur at stresses lower than the Orowan stress but the data shown in Figure 7 suggest that the Orowan stress represents a threshold value

below which creep of dispersion strengthened single crystals will not occur.

3) At constant $\dot{\epsilon}_s/D$, the creep strength of the dispersion strengthened single crystal can be expressed as the sum of the creep strength of a polycrystalline matrix and the Orowan stress.

$$\left(\frac{\sigma}{E}\right)_{Ni_{20}Cr_2ThO_2} = \left(\frac{\sigma}{E}\right)_{Ni_{80}Cr} + \left(\frac{\sigma}{E}\right)_{Orowan} \qquad (3)$$

From this equation, it appears that the creep rates for single crystal TD-nichrome are fully compatible with those of the nichrome matrix provided that comparisons of the effective stress vice the applied stress are made. The effective stress is then written as:

$$\sigma_e = \sigma_a - \sigma_b \qquad (4)$$

Where σ_a is the applied stress and σ_b is the Orowan bowing stress for the dispersion strengthened material. Replacing σ_a with σ_e in the power law equation, would then yield n values in the 5 to 6 range.

It was also seen in Cr, Mo, V steel that the n value from a creep rate vs. stress plot, changed gradually from 14 to 1. This shown in Figure 8 which is again plotted against applied stress. Other approaches to the problem of creep in particle

hardened materials are due to Edwards et al [ref 13] and Oliver and Nix [ref 14]. In the former approach, the particle/matrix interface was modelled as a dislocation source while in the latter, solute drag effects on dislocations bowing through dispersoids, are considered.

E. SCOPE OF PRESENT WORK

1. Previous work on FVS1212

Franck and Hawk [ref 8] conducted a study of FVS1212 and obtained the results shown in Figure 9. There, diamond pyramid hardness (DPH) is plotted vs. annealing time and shows no significant change in the hardness of the sample annealed at 500°C for up to 100 hours. This suggests no significant change in the microstructure i.e., little or no coarsening. Pharr and co-workers [ref 15] have performed constant stress creep tests over the temperature range of 237°C to 479°C on FVS1212. The creep properties, i.e., steady state strain rates as a function of stress are shown in Figure 10. This figure, which is plotted against applied stress, shows the stress exponent to range from n = 13 to 32 as one would expect to see in a dispersion strengthened alloy without correcting for the Orowan bowing stress σ_b. Work on this same alloy by Benci and Frazier is shown in Figure 11 [ref 16]. The response of FVS1212 at 371°C indicates that there can possibly be more than one n value for a specific temperature,

indicating that there may be different creep mechanisms at work, at different stress levels.

2. Objectives of this study

This investigation will focus on the constant stress creep behavior of FVS1212 at stress levels between 70 MPa and 150 Mpa and temperatures of 350 to 450°C. Values of n and Q_c will be obtained and correlated to possible mechanisms of creep. Furthermore, constant strain rate tension test will also be performed on the alloy at rates of 6.56×10^{-5} sec^{-1} and 6.56×10^{-6} sec^{-1}, from room temperature to 400°C. The focus of these tests will be to observe the mechanical property variations with temperature at the two strain rates used. The properties of interest are yield stress, % elongation, and the strain rate sensitivity of the yield strength. Microscopy of the fracture surfaces will also be used to correlate with the mechanical behavior. Finally, transmission electron microscopy will be used to study the microstructure of the as received and crept sample to observe dislocation structure and particle cutting, if any.

III. EXPERIMENTAL PROCEDURE

A. MATERIAL PROCESSING AND FABRICATION

The aluminum alloy used to conduct this investigation was obtained from Allied Signal Corp, Morristown, N.J. The material's commercial name is FVS1212 its composition is Al-11.7%Fe-1.2%V-2.3%Si and it contained 36% dispersoids by volume [ref 15]. It was developed to meet the needs of applications requiring superior ambient and elevated temperature strength and stiffness [ref 17].

Through rapid solidification processes (melt spinning/ planar flow casting) cast ribbons of the material were produced. These cast ribbons were then pulverized to provide the feed material for powder metallurgy (PM) vacuum degassing and canless hot pressing to produce billets. These billets were then extruded at a ratio of 14:1, to produce the final product form.

B. CONSTANT STRESS TESTS

1. Creep testing machines

The two test machines used to perform the constant stress test were machines designed at Naval Postgraduate School (NPS) and patterned after machines built by Barrett and later modified by Matlock [ref 18]. A diagram of the constant stress creep test unit is shown in Figure 12. The machines

were designed to transmit loads ranging from 15 to 222.5 Newtons (0.3 to 50 lbs.) at strains as high as 300 percent. To maintain a constant stress an Andrade-Chalmers lever arm was used. As the sample elongates (i.e., as cross sectional area decreases) the lever arm rotates inward decreasing the effective moment arm, thus decreasing the applied load and maintaining a constant stress. The assumption that the load train is rigid and that the linkage displacement is taken up uniformly, was made when designing the arm. The contour of the arm was designed using AUTOCAD software in conjunction with a graphical technique developed by Coghlan [ref 19]. The design assumed that the effective test sample gauge length was 12.7 mm (0.5 in.) and utilized an initial lever ratio of 10:1. The lever arm was constructed of 2024-T6 aluminum 6.4 mm (0.25 in) thick and attached to a shaft which rotates on a set of precision bearings. An adjustable counterbalance was attached to the other end of the shaft. Fixed weights (used to counterbalance the load train), in conjunction with the adjustable counterbalance weights on the shaft, were used to ensure that the sample only sensed the applied load.

Sample elongation was measured using a Schaevitz linear variable differential transformer (LVDT) with a 25.4 mm (1.0 in.) displacement. The output signal (2.866mV/V) from the LVDT was conditioned by a Schaevitz ATA101 analog transducer amplifier. The voltage was then measured by a

Hewlett-Packard (HP) 3497A Data Acquisition unit which was controlled by a HP 9826 computer.

Astro tubular furnaces, model A237S, rated at maintaining temperature up to 1200°C, were used to maintain the various test temperatures. To control and monitor the furnaces, Eurotherm 808 digital temperature controllers were used.

The tensile test samples that were used in the constant stress test units were cut to the dimensions shown in Figure 13. The grips (Figure 14) used to hold the test samples in the machines were special self-aligning grips, manufactured by Collins Instrument Company, Freeport, Texas. The grips were fabricated from Inconel alloy 625 and were machined using a wire electro-discharge process to control tolerances.

2. Software

The software used in conjunction with the creep test was written in HP basic 2.0 and was last modified by Goodson [ref 18]. The software was designed to control both creep machines simultaneously and provide a real-time display on the video monitor of the HP 9826 of engineering strain vs. time of both test. The algorithm was written to sample 5000 voltages during each test and convert the voltages to engineering strain. Upon completion of the tests the user could look at the plot of each test, either true or engineering strain vs.

time, on the video monitor of the HP 9826 or plot them on the HP 7470A plotter. All the data files were stored on 5 1/4 double density disks.

3. Constant Temperature Creep Testing

Upon allowing the furnaces to stabilize to the desired temperature, the furnace was lowered to insert the grip assembly into the notched grip holders. Upon carefully installing the grip assembly into holder and removing all the slack, a small load was placed on the monel strap attached to the lever arm to prevent slippage of the grip assembly in the grip holder while returning the furnace to its test position and waiting for the temperature to re-stabilize back to the desired temperature. Once the furnace was returned to its test position it normally took between 30 - 40 minutes for it to re-stabilize. During this time the required test parameters were entered into the computer and the weight which was required for the desired stress was calculated. Once the temperature stabilized the remaining weight was added to each machine and the program started. Test times ranged from 45 minutes to 96 hours. All testing was conducted between 350 and 450°C.

C. CONSTANT EXTENSION RATE (TENSION) TEST

The constant extension rate test or constant cross-head speed test were conducted on an Instron, model 6027, mechanical testing machine with a 200 kN calibrated load cell.

The testing temperatures ranged from room temperature to 400°C. These temperature were maintained by a Marshall clamshell furnace model 2232. The same self-aligning grips that were used on the constant stress tests were also used on the constant extension test. After the furnace had stabilized to the desired temperature, it was de-energized, opened and the grip assembly inserted into the grip holders and slack removed. The furnace was then closed and re-energized. Once the furnace re-stabilized to the desired temperature the test was started and a real-time plot of stress vs. displacement was obtained.

D. MICROSCOPY (TEM AND SEM)

1. Scanning Electron Microscopy

Various test samples were examined in the Cambridge Stereo Scan S200 scanning electron microscope to observe the fracture surfaces after tension tests.

2. Transmission Electron Microscopy

Other selected test samples were ground down to approximately 150 μm and from these samples 3 mm disks were punched. These disks were then further thinned until a small hole appeared in the center. Thinning was done by electrochemically polishing the sample on a Struers Tenupol electropolishing device using a 6% perchloric acid, 59% methanol and 35% butyl alcohol solution, cooled to -40°C with liquid nitrogen. The disks were then examined in a JEOL

Model JEM-100CX II, Transmission Electron Microscope operating at 120 kV.

E. X-RAY DIFFRACTOMETRY

As received material was pulverized using a ceramic mortar and pestle. The powder was then placed on an glass slide and held in place using amyl-acetate. X-ray diffraction was obtain from a Phillips x-ray generator, XRG-3100, controlled by a Phillips diffractometer control unit, PW-1710. The generator was operated at 30 kV and 35 mA.

IV. RESULTS AND DISCUSSION

A. CONSTANT EXTENSION TEST.

The temperature selection for the Instron tests ranged from room temperature to 400°C. The strain rates were 6.56×10^{-6} sec $^{-1}$ (.005 mm/min crosshead speed) and 6.56×10^{-5} sec^{-1} (.05 mm/min). Figure 15 is a representation of the stress vs. plastic strain of the room temperature and 400°C tests. The reason for omitting the elastic region was to eliminate any contribution to the elastic deformation of the sample from the machine and grips; and due to the lack of an extensiometer to measure exact sample elongation. From the curves and the samples, the following points are noted;

1) At room temperature and 400°C there is only a small separation between the yield stress and the ultimate tensile strength (i.e., a small strain hardening range).

2) The room temperature samples appear to have higher values of strain hardening exponent, than the 400°C samples. The 400°C samples show large, flat region in the stress/strain plot, which is typical of particle hardened alloys where dislocations climb over the particles [ref 20].

3) Prominent necking is seen on the samples that were tested below 150°C.

The mechanical behavior of this alloy appears to go through a transition at around 250°C. Figure 16 shows the stress vs. plastic strain for the 250°C tests. In this case there is a much larger strain hardening region which appears to diminish with increasing temperature. The large flat regions seen at the higher temperatures (above 250°C) occur during creep type deformation and facilitates thermally activated dislocation climb over the particles. At the lower temperatures, dislocation bowing would appear to be the operative mechanism and this mechanism appears to explains the small but steep strain hardening region. This range is short due to plastic instability that leads to neck formation.

Figure 17 is a micrograph of the room temperature sample fracture surface, tested at 6.56×10^{-5} sec^{-1}. There is no evidence of plastic flow of the matrix around the dispersoids and the fracture appears to be intergranular. Figure 18 is from the 400°C sample tested at 6.56×10^{-5} sec^{-1}. Here dimple formation, typical of ductile fracture can be seen. Matrix flow and necking around the dispersoids is evident. At 250°C, the fracture surface appears quite different from the previous micrographs. This is shown in Figure 19, where step like features similar to microcleavage planes are evident. These microcleavage steps were not seen on any other fracture surface, and can be associated with the transition from low temperature behavior bowing to high temperature dislocation climb. The extended dislocation activity, as evidenced by

large strain hardening region at 250°C can lead to the formation of dislocation forests that would locally increase stress concentration and lead to failure along these planes giving the appearance of cleavage steps.

Figures 20 and 21 summarize the results of the tests conducted at 6.56×10^{-5} sec^{-1} and 6.56×10^{-6} sec^{-1}. The plots contain both the yield stress (0.1%) vs. temperature and 0.4% flow stress vs. temperature. It appears that there are two plateaus, one at around 75 - 100°C and a second one around 250 - 300°C in both figures. Previous data from a similar dispersion strengthened alloy with less iron, FVS0812, also displayed a plateau [ref 9]. In the FVS0812 alloy the plateau appears between 75 - 150°C, at a strain rates of 8.89×10^{-5} sec^{-1}. The % elongation vs. temperature of FVS0812 indicated a drop in elongation in the region of the plateau [ref 9]. These plateaus are normally associated with some type of strengthening mechanism occurring during the test, and has been attributed to dynamic strain aging [ref 9, 10].

In Figures 20 and 21 it should also be noted that even at the 0.4% flow stress the plateaus are still visible and that the difference between the 0.4% flow stress and the yield stress is at a maximum at around 200°C, indicating large strain hardening regions. Figure 22 plots one measure of the strain hardening in the form of a stress difference vs. temperature. A higher stress difference between the 0.4% and the 0.1% flow stress indicates a steep slope and effective

strain hardening, although at the higher temperatures, the 0.4% flow stress is already close to the ultimate tensile stress. From this data it can be seen that 200 - 250°C marks a transition in the mechanical behavior of FVS1212, as similar plots were obtained at both the strain rates used.

The % elongation of the sample vs. temperature is shown in Figure 23. Here it can be seen that a minimum in ductility exists between 100 - 250°C, which coincides with the plateaus in yield stress. The high % elongation at the lower temperatures is primarily due to the neck formation while at higher temperatures, elongation is due to dislocation climb over the barriers. Once again, at around 250°C, the ductility begins to improve. This can be attributed to a change in deformation behavior.

Strain rate sensitivity vs. temperature is also plotted, in Figure 24. The strain rate sensitivity (m) is defined as;

$$m = \frac{\log \frac{\sigma_2}{\sigma_1}}{\log \frac{\dot{\varepsilon}_2}{\dot{\varepsilon}_1}} \qquad (5)$$

and is based on the following behavior:

$$\sigma = C \cdot \dot{\varepsilon}^m \qquad (6)$$

The yield strength values were used to obtain the graph in Figure 24. Two dips appear in this graph with the major dip appearing at 250°C. The calculated m for this temperature turned out to be negative, since the yield stress for 6.56 x 10^{-5} sec^{-1} was lower than that of 6.56 x 10^{-6} sec^{-1}, i.e., 190 MPa and 211 MPa, respectively. Earlier work on other particle hardened materials, for example 30 volume % Al_2O_3 in a zinc matrix, showed that a negative m can exist and that this region is dispersion weakened (i.e., weaker than the unreinforced matrix) [ref 13].

Due to the dip in ductility and the strain rate sensitivity, it was decided to further investigate the behavior of the alloy at 250°C. The additional crosshead speeds that were selected were 0.01 mm/min (1.3 x 10^{-5} sec^{-1}) and 0.1 mm/min (1.3 x 10^{-4} sec^{-1}). Figure 25 shows yield stress 0.4% and 0.8% flow stress vs. strain rate at 250°C. Yield stress appears to go through a maximum and then drops with increasing strain rate. This is indicative of a weakening behavior with increasing strain rate. The 0.4% and 0.8% flow stress curves appear to deviate from this behavior at the higher strain rates and show an increase in the flow stresses indicating a larger range of strain hardening at the higher strain rate. Figure 26 shows % elongation and stress difference vs. strain rates for the samples at 250°C. The strain hardening range shown by the stress difference (0.4% - yield stress) curves appears to be relatively constant (with

a slight increase) up to a strain rate of 6.56×10^{-5} sec^{-1} after which there is a marked increase indicating once again the high strain hardening at the higher strain rate. The drop in ductility at 1.3×10^{-4} sec^{-1} coincides with the increased strain hardening observed at that strain rate. It would appear that strain rate has a pronounced effect on the mechanical behavior of FVS1212 at a temperature of 250°C.

B. CONSTANT STRESS CREEP TEST

In this portion of the research, samples were tested at different temperatures (350°,400°,425°, and 450 °C) and different stresses (70 MPa to 150 MPa). All tests were run up to 96 hours or until failure of the sample which ever came first. Steady state creep rates were measured from the slope of the curves during secondary creep. Figure 27 is a typical curve of true strain vs. time. As seen in the figure, the creep curve exhibits three distinct portions. The primary stage is characterized by a rapid initial strain rate which subsequently decreases until the secondary stage is reached. The secondary stage is characterized by a steady state creep rate which remains constant. The tertiary stage is characterized by an accelerated creep rate which continues until failure of the sample. At this stage micro-void formation and micro-necking occurs.

Steady state creep rates were calculated for all the tests and the 'log' of these creep rates are plotted vs. 'log' of

the stress in Figure 28. Also included in Figure 28 are some results that were obtain from previous work on FVS1212 [ref 15], at 401°C and 479°C. The data obtained during this investigation at 400 °C, appears to be consistent with the data obtained by Pharr et al [ref 15] at 401°C. Another point of interest is that there is a change in the slope in the 400°C and 425°C lines. The slope of the lines in Figure 28 should give the value of n, the stress exponent. Stress exponents for pure metals and single-phase alloys usually ranges from 2 to 4 and 4 to 6, respectively, although values of n greater than these have been found in other particle strengthen alloys (up to 70). This is normally associated with high stress levels (i.e., $\sigma > 10^{-3}$ E) where it is believed that the power law breaks down in dispersion strengthened materials which exhibit a threshold stress in their creep behavior [ref 12]. The calculated n values from Figure 28 ranged from 3 to 16. The break in the slope of the tests run at 400°C and 425°C has also been noted in other particle hardened alloys [ref 12] and has been variously reported as an abrupt change [ref 12] or a gradual one [ref 12]. In this investigation the break appears to occur at half the yield stress determined at strain rates of $\approx 6.56 \times 10^{-5}$ sec^{-1}. The apparent breakdown of the power law cannot be attributed to macroscopic yielding.

In an attempt to evaluate the activation energy for creep, Q_c, from the results of the constant stress test, steady state

creep rates vs. 1/T are plotted in Figure 29. If we can assume that the dislocation structure is independent of temperature during steady state creep (i.e., at any specific temperature, the dependence of the structure is only on stress), then the slope of the strain rate vs. 1/T (log - log plot) line should correspond to the activation energy according to the relationship:

$$Q_c = -R\left(\frac{\ln \frac{\dot{\epsilon}_2}{\dot{\epsilon}_1}}{\frac{1}{T_2} - \frac{1}{T_1}}\right) \times 2.3 \qquad (7)$$

The factor of 2.3 is included to account for the conversion from a log strain rate vs. 1/T plot to a ln strain rate vs. ln [exp(Q/RT)] slope. This equation is derived from the standard power law relationship used in the analysis of stress and temperature dependence of creep. The highest activation energy calculated was approximately 1000 kJ/mole, but as stress and temperature decreased so did the value for activation energy. The lowest value calculated was approximately 100 kJ/mole. This appears to indicate that there are various mechanisms at work, although the values lead to one primary mechanism at high stresses and temperatures.

Figure 30 shows a plot of steady state creep rate (temperature compensated using the activation energy for self diffusion in aluminum) vs. the log of stress (modulus

compensated) and includes data obtained by Pharr et al [ref 15]. It appears that there is a threshold stress. This implies that no creep will occur if the applied stress is below the threshold level. If there is an actual threshold stress, then the effective stress under which creep occurs should be written as;

$$\sigma_e = \sigma_a - \sigma_{th} \tag{8}$$

and the power law equation can modified accordingly;

$$\dot{\varepsilon} = K\left(\frac{\sigma_a - \sigma_{th}}{E}\right)^n \exp\left(-\frac{Q_c}{RT}\right) \tag{9}$$

With respect to the dispersion strengthened alloys, this threshold stress has been proposed to be the Orowan bowing stress σ_b. The apparent weakness with this theory is the ability of dislocations to climb over the particles at the temperatures involved, even at stresses below the threshold or Orowan bowing stress, leading to observable creep deformation. However, if one considers the high volume fraction of dispersoids (≈ 36%) it is possible that immediately after climb, the dislocations encounter obstacles again and if stresses below the bowing stress are used, then the material can exhibit a threshold stress for creep. Using the threshold stress idea, values of n would now approach the values expected for creep of the matrix material under equivalent

test conditions [ref 12], [ref 15]. It appears from Figure 31, that the threshold stress that is approached at low creep rates occurs $\approx 7 \times 10^{-4}E$ (in GPa). For the temperature range of 400° to 450°C, this implies a threshold stress of 50 to 56 MPa, respectively.

With regard to activation energy, it has been shown that if an accurate value for the activation energy is selected, creep data obtained at various temperatures and stress levels should coincide on a single plot of normalized creep rate vs. modulus compensated stress [ref 15]. Initially values of E for the different temperature had to be determined, since E is known to vary with temperature [ref 1]. The first attempt to plot the normalized creep rates vs. modulus compensated stress is shown in Figure 30. An activation energy of 142 kJ/mole was selected, since it is the activation energy for self-diffusion of aluminum. The plot did not produce a single curve, so various activation energies were attempted in order to obtain the desired single curve. From these attempts, it appears that an activation energy of around 400 kJ/mole produced the best fit of the data, Figure 31. Although, it is also noted that there was a range around 400 kJ/mole that also provides results that are nearly as good as the one obtained with the 400 kJ/mole value.

V. CONCLUSIONS

A. CONSTANT EXTENSION RATE (TENSION) TEST

It appears that fracture behavior at low temperature (up to around 150°C) is characterized by necking due to plastic instability. Fracture surfaces of these samples (up to 150°C) appear intergranular and did not show any evidence of gross plastic flow in the matrix. Most of the elongation measured at these temperatures can be attributed to necking. At temperatures above 250°C the deformation behavior changed and large flat regions in the stress vs. strain plots were observed. The fracture surfaces of these samples showed plastic deformation.

At 250°C the fracture surface appeared different. There were ledges (micro-cleavage planes) observed on the fracture surface. Ductility appeared to be at a minimum around 200 to 250°C. Earlier work on a similar aluminum alloy (FVS0812) also noted a ductility trough in the ductility vs. temperature plot. This was associated with a phenomena that is commonly observed in aluminum alloys at room temperature, called dynamic strain aging. FVS0812 exhibits this phenomena at around 150°C and it is believed to occur due to the presence of iron in solution [ref 10, 11]. It has been noted that a drop in strain rate sensitivity, m, occurs in the same

temperature range where ductility is at a minimum and yield strength plateaus are observed. This was also seen in FVS0611 and FVS0812 alloys where these dips in m were associated with the DSA phenomena. The temperature range of DSA shifted to the right (i.e., an increase in temperature) with increased alloy content from FVS0611 to FVS0812. The only difference between these two alloys was an increase in the alloy content, in particular the iron content (an increase from 6% to 8%). It has also been shown that the drop in strain rate sensitivity is much more severe for dispersion strengthen materials than for solid solution materials, in the temperature ranges where the DSA phenomena occurs [ref 10]. In fact in certain cases a negative value for m has been reported, and this has been associated with dispersion weakening [ref 13]. It is conceivable that the phenomena that was observed in FVS0611 and FVS0812, specifically DSA could lead to a ductility trough and drop in strain rate sensitivity of FVS1212 at temperature i.e., centered around 100°C. At 250°C however, the drop in m may or may not be attributed to any DSA activity since the highest activation energy for diffusion in aluminum is that of iron (in this alloy), which is already responsible for a dip in m at ≈ 150°C in FVS0812. Two possibilities exist here: i) The higher alloying elements and increase in dispersoid volume have shifted the DSA effect, due to iron, to a higher temperature in FVS1212; or ii) The dip in m is associated with a totally different mechanism.

It appears then, that 250°C is the temperature at which deformation behavior changes with respect to dislocation motion.

In further testing at 250°C different strain rate tests showed anomalous behavior in the strain rate vs. stress plots. At high strain rates a drop in yield stress was observed between 1.3×10^{-4} sec^{-1} and 1.3×10^{-5} sec^{-1}. Strain hardening at the higher strain rates appeared to increase when compared to strain hardening behavior of the same alloy at 250°C at slower strain rates. No other fracture surfaces (except those tested at 250°C) showed the micro-cleavage features and while the sample tested at the highest strain rate (1.3×10^{-4} sec^{-1}) appeared to have small dimples in the side walls of the micro-cleavage features of the fracture surface. This is consistent with the large plastic deformation regions seen in the stress vs. strain plot at that strain rate. In seeking a satisfactory explanation for the yield stress behavior at 250°C with the strain rate, it is suggested that the interaction of the dislocations with the solute atmosphere of iron is responsible for the low value of m. At faster strain rates, diffusion of iron to the dislocations, that spend less time waiting at the dispersoid, is not fast enough to show an effective increase in yield stress. Thus, yield stress is not effected by this strengthening mechanism and leads to a drop in the stress level at which dislocations become mobile. This enhanced dislocation mobility is also responsible for the

large strain hardening region at this temperature. Above 250°C, dislocation climb becomes easier, thereby limiting the extent of the strain hardening region.

From the constant strain rate tests in this investigation, it is shown that this alloy exhibits a ductility trough at around 250°C which is also the temperature which appears to separate the low temperature and high temperature deformation behavior. Strain rate sensitivity values (using yield stress) obtained at 250°C have shown extremely small positive numbers and even some slightly negative values. These effects can be tentatively attributed to the presence of iron in the matrix and are due to DSA in FVS1212 at 250°C. The dip in m at ≈ 100°C can be attributed to silicon or vanadium in solution in the matrix.

B. CONSTANT STRESS TESTS

Constant stress data indicates various values for the stress exponent n (based on the power law of creep). The n values calculated ranged from 4 to 16. Dispersion strengthened materials are known to exhibit high values of n and are commonly treated as materials with a threshold stress. This threshold stress is believed to be the stress required to bow out a dislocation between two dispersoids, leaving behind a dislocation loop surrounding the dispersoid particles and effectively reducing the interparticle spacing. This has been used to physically explain the increased value of n at higher

stress due to the increase in the threshold stress derived from the decrease in interparticle spacing. Hence the effective stress under which dislocation creep occurs is very different from the applied stress, especially at high levels of stress. If this holds true then the materials should show a threshold stress below which no creep occurs.

From the data obtained in this investigation, when plotting steady state creep vs. stress a threshold stress may exist at a value of stress/E of 7×10^{-4}. Using the idea of Orowan bowing as the threshold stress, a value of 440 MPa is obtained for an interparticle spacing of 250 Å and a shear modulus of 20 GPa at 400°C. This does not compare well with the 50 - 56 MPa measured in Figure 31. The value of 440 MPa is based on the assumption that the dispersoids are uniformly distributed and are of uniform size. When strain rate vs. 1/T is plotted for different stress levels, the slope at the higher stress and temperatures gives an activation energy for creep around 960 (± 50) kJ/mole. The assumption made in representing the data in this fashion and extracting an activation energy is that the structure is a function only of stress. Evidently this is not the case as can be seen from plots of 70 MPa and 80 MPa where a range of activation energy exist from 100 kJ/mole to 950 kJ/mole. At low temperatures (0.08 to 0.27Tm), the activation energy for creep in pure aluminum ranges between 20 and 110 kJ/mole. This sort of behavior has been attributed to a dislocation intersection of

mechanisms. This is not the case in FVS1212, and a satisfactory explanation for the abnormally high activation energy is still being sought. The high end activation energy calculated from this investigation is larger than the activation energy for diffusion of any of the alloying elements in solution. Table (I) list the activation energy for diffusion of the alloying elements in aluminum [ref 21].

Table I

Aluminum	Iron	Vanadium	Silicon
142 kJ/mole	257 kJ/mole	82 kJ/mole	159 kJ/mole

Iron (Fe) appears to have the highest activation energy, although it is still much lower than the highest calculated activation energy. It appears that the presence of a large fraction of planar defects (i.e., interfaces) and the presence of stress in matrix could all contribute to an effective reduction of the activation energy of these elements thereby further removing their values from those calculated for creep in FVS1212. Another technique for obtaining the activation energy is to plot the log of temperature-compensated strain vs. log of modulus compensated stress using an appropriate value of activation energy in the temperature compensation of strain rate. When this was done, it was found that the data

nearly coincided on one single curve with an activation energy of ≈ 420 kJ/mole (± 20 kJ/mole). These activation energies are still higher values than the diffusion of Fe, V, and Si in aluminum. Using the concept of threshold stress, it has been shown that by modifying the stress for creep one can actually decrease the values for n and Q_c [ref 12], [ref 15]. No attempt was made in this study to plot strain rate vs. effective stress and to obtain the new activation energy in this manner.

TEM investigation of microstructure of as received and as crept samples showed a relatively low density of dislocations with no evidence of particle cutting at low temperatures. An earlier theory [ref 15] designates the particle matrix interface as an effective dislocation source. These materials generated many dislocations which could move short distances before being consumed once again at the particle interface. This does not appear to be the case in FVS alloys, since it has been shown that the dispersoid/ matrix interface has a relatively high degree of coherency, thereby making it a poor dislocation source. The absence of dislocation loops around the dispersoids in the TEM investigation suggest that extensive Orowan looping does not occur, although active dislocation sinks at the particle/matrix interface can account for their absence too. Consequently, the decrease in the interparticle spacing is minimal, and no change in the bowing stress occurs with deformation.

From the preceding discussion it can be seen that the calculated activation energy thus represents a combination of mechanisms. TEM shows an absence of dislocation bowing and looping which tends to suggest either i) limited dislocation activity, or ii) effective dislocation sinks becoming operational. Owing to the high n values it is concluded that dislocation sinks were effectively annihilating the dislocation structure.

Overall, this material shows a threshold stress ($\approx 7 \times 10^{-4}E$), goes thru a transition in n and activation energies for creep; and displays an activation energy that is much higher than any of the activation energy values for diffusion of Fe, V, or Si in an aluminum matrix.

APPENDIX A. FIGURES

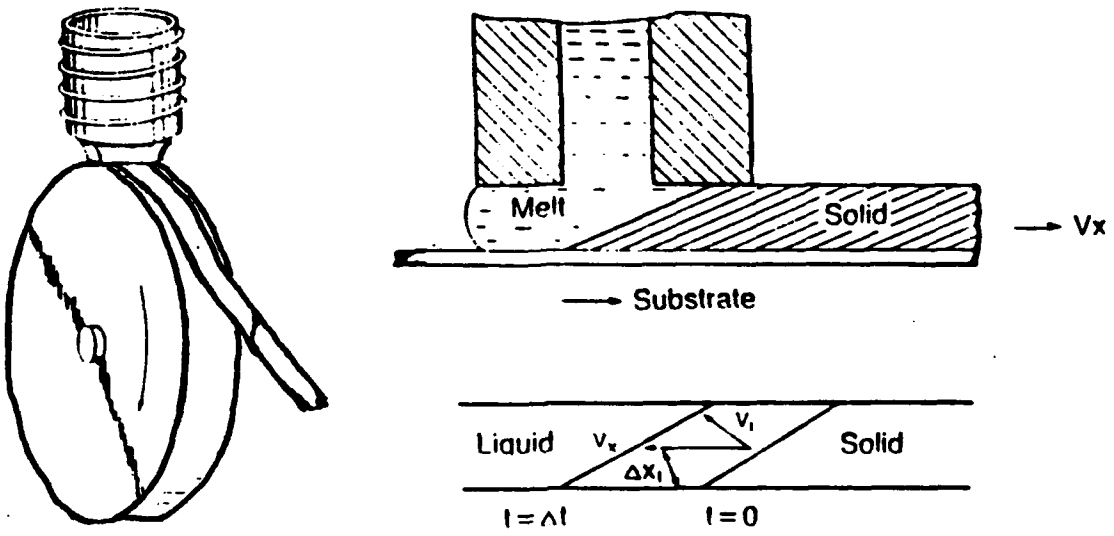

Figure 1. Schematic of the planar flow casting process [ref 2].

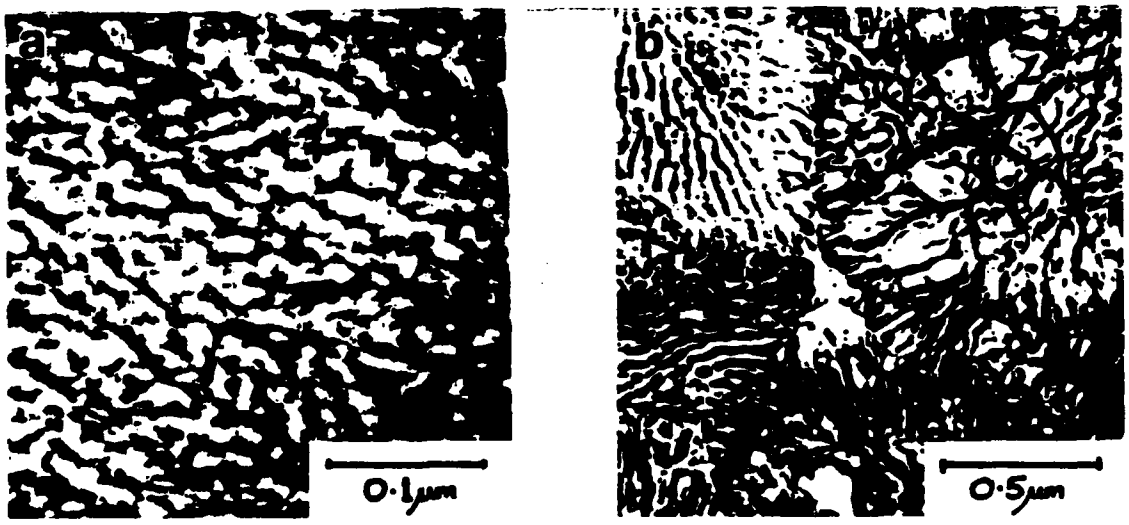

Figure 2. Transmission electron micrographs of Al-12wt%Fe rapidly solidified alloy showing (a) zone A and (b) zone B microstructure [ref 2].

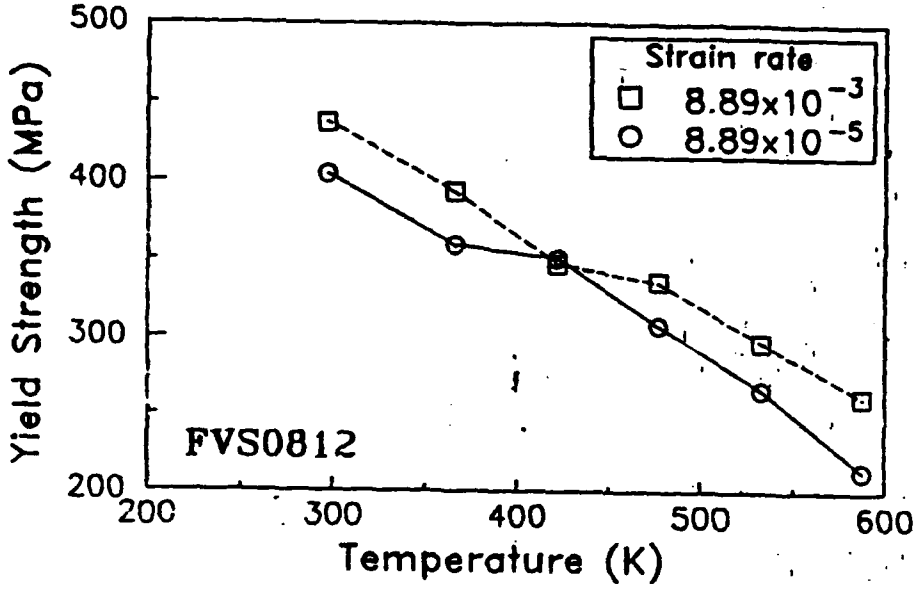

Figure 3. Yield stress vs temperature for alloy FVS0812 at strain rates of 8.89 x10^{-5} sec^{-1} and 8.89 x10^{-3} sec^{-1}. Note plateau in curves between 80°C and 200°C, depending upon strain rates [ref 9].

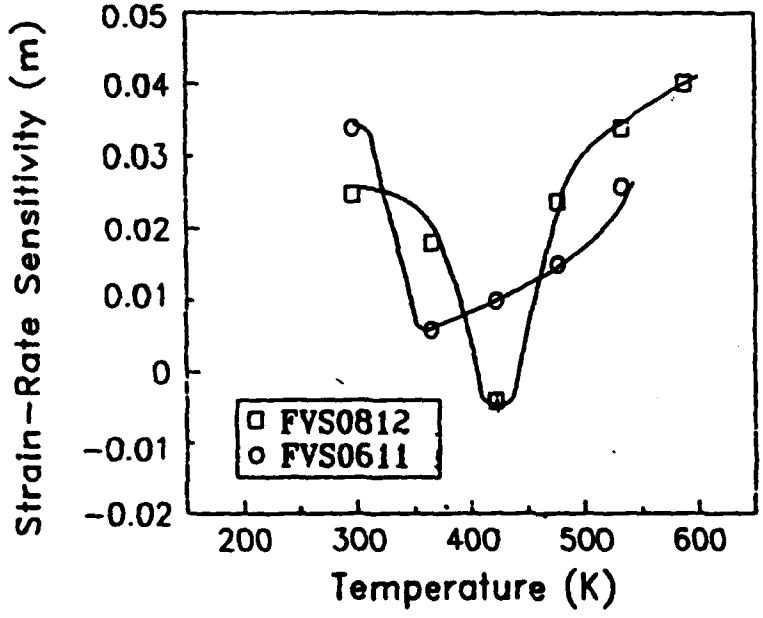

Figure 4. Strain rate sensitivity (m) vs temperature for alloys FVS0611 and FVS0812. Note dip in m at 75°C and 150°C, respectively [ref 9].

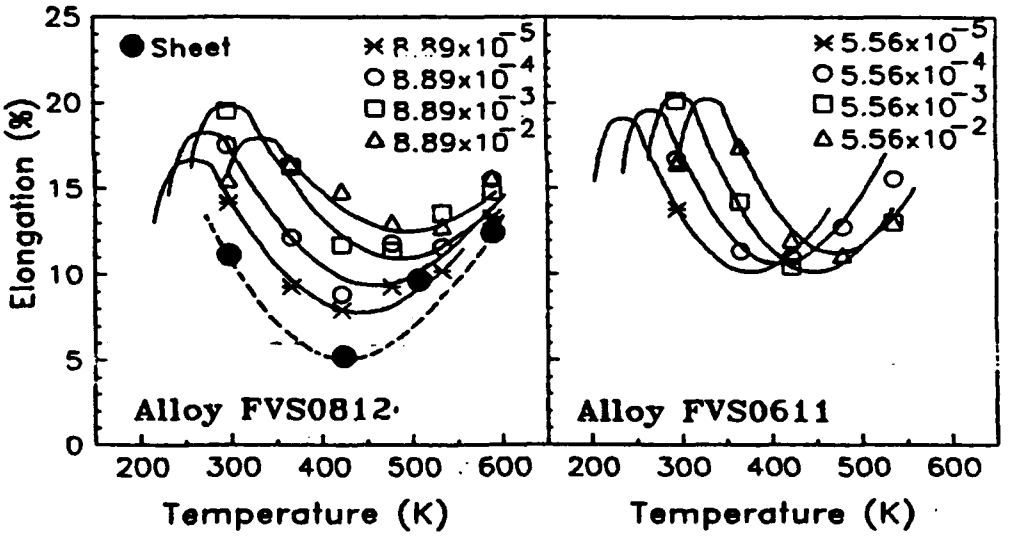

Figure 5. Elongation vs temperature for alloys FVS0611 and FVS0812 at various strain rates. Note dip in ductility, at low strain rates corresponding to dip in m in figure 4 [ref 9].

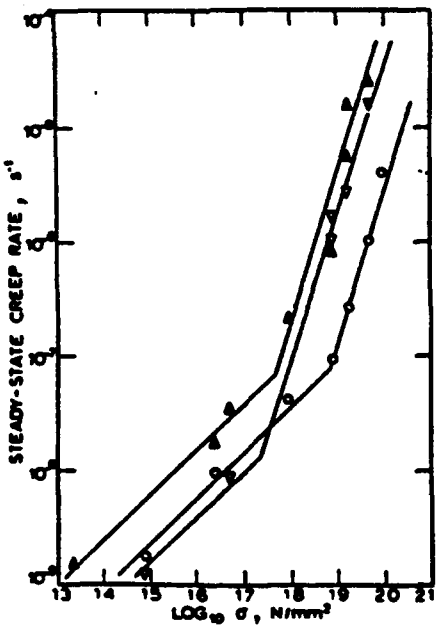

Figure 6. Stress dependence of secondary creep rate of copper-0.88wt% cobalt with particle diameter of 3.3 nm (▲), 8.3 nm (o)and 17.2 nm (▽). Note drastic change in slope from n = 12 to n = 5 [ref 12].

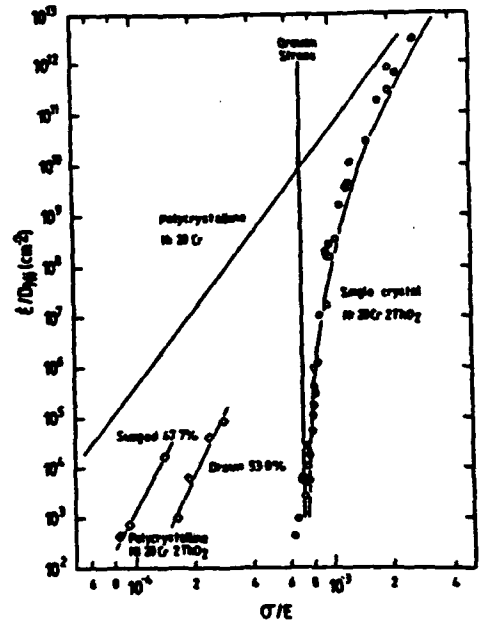

Figure 7. Diffusion compensated creep rate vs modulus compensated stress for single phase nickel-20% chromium and for single crystals and polycrystals of TD-nichrome [ref 12].

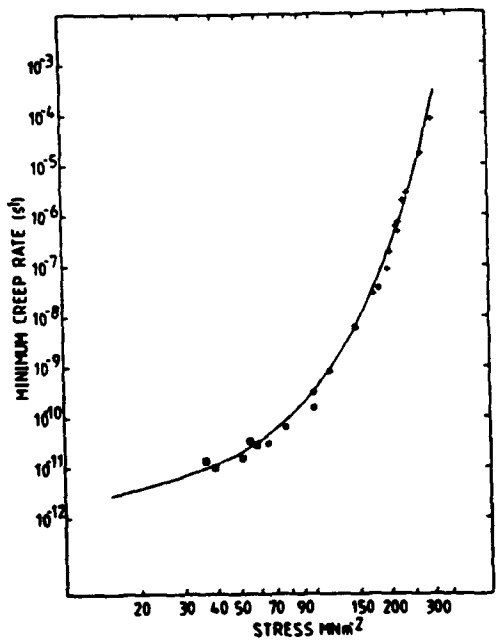

Figure 8. Minimum creep rate vs stress for Cr, Mo, V steel at 838 K. Note gradual change in slope between high stress and low stress region [ref 12].

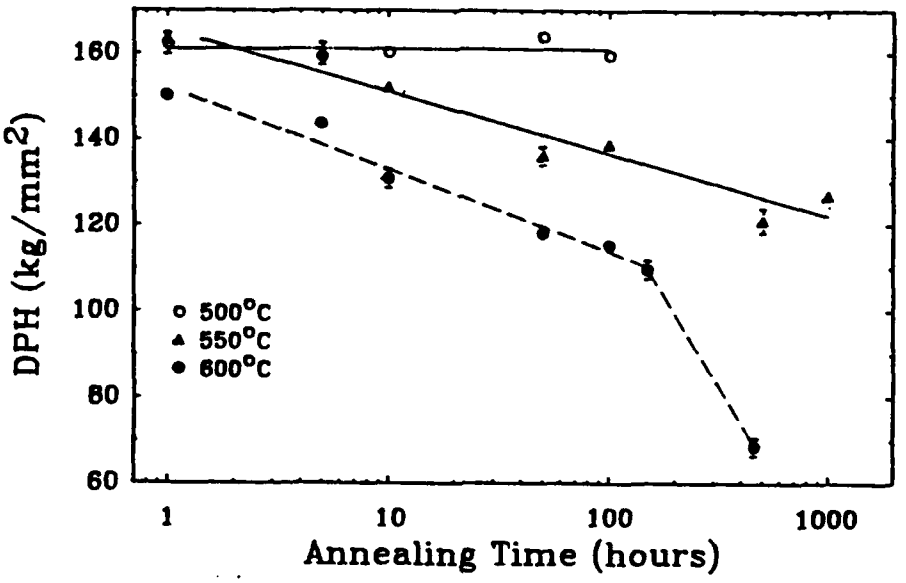

Figure 9. Room temperature diamond pyramid hardness (DPH) vs annealing time at 500°C. Note, no observable change in DPH for sample annealed at 500°C for 100 hours [ref 8].

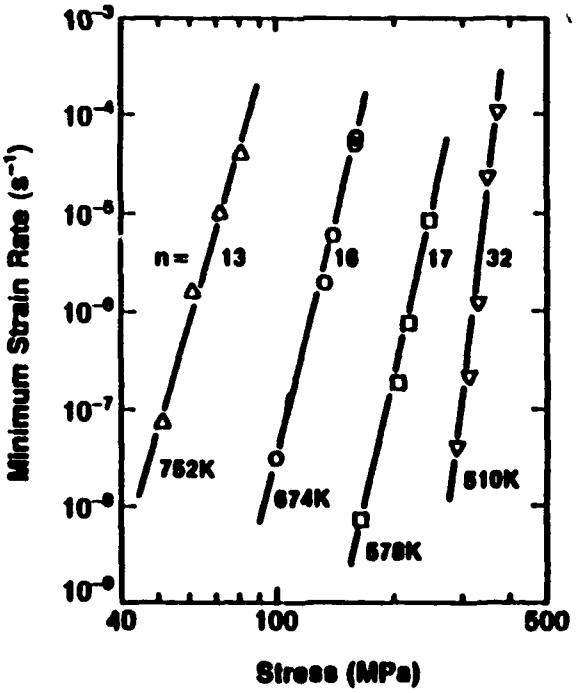

Figure 10. Minimum strain rate vs stress for FVS1212 [ref 15].

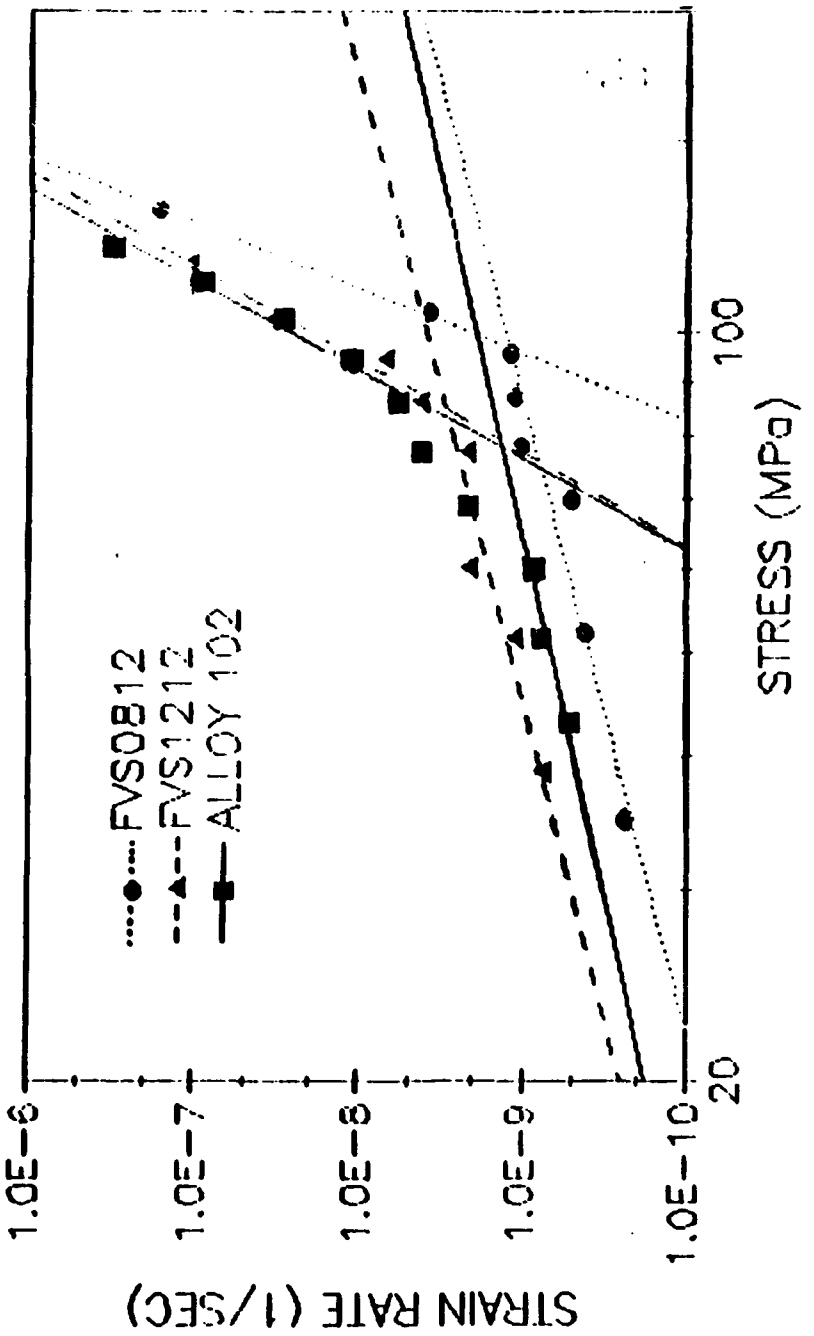

Figure 11. Minimum strain rate vs temperature for FVS1212 and FVS0812. Note sharp change in n [ref 16].

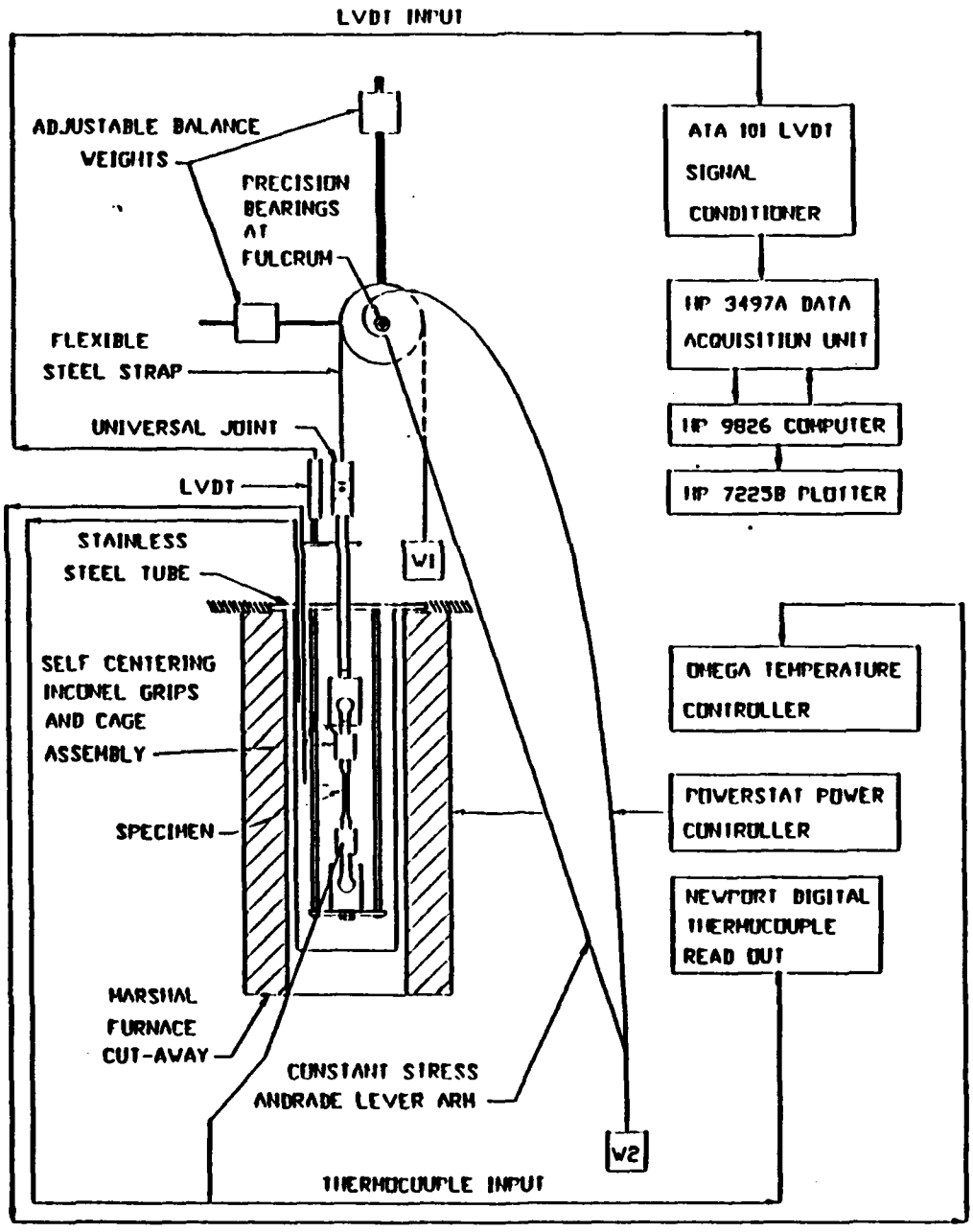

Figure 12. Schematic of Constant Stress Creep Apparatus.

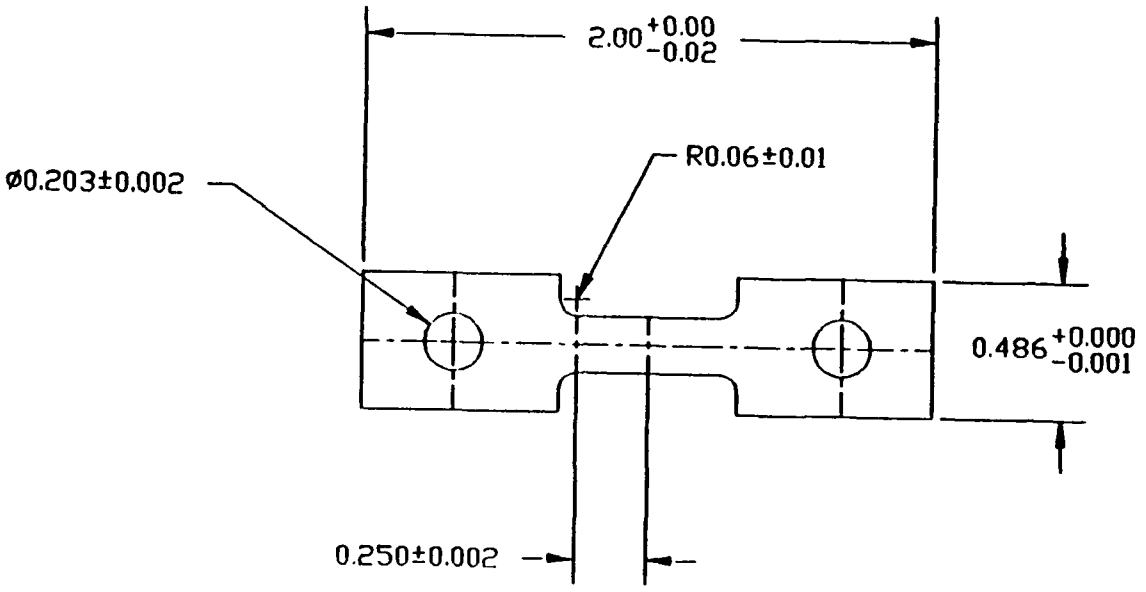

Figure 13. Sample geometry for creep test.

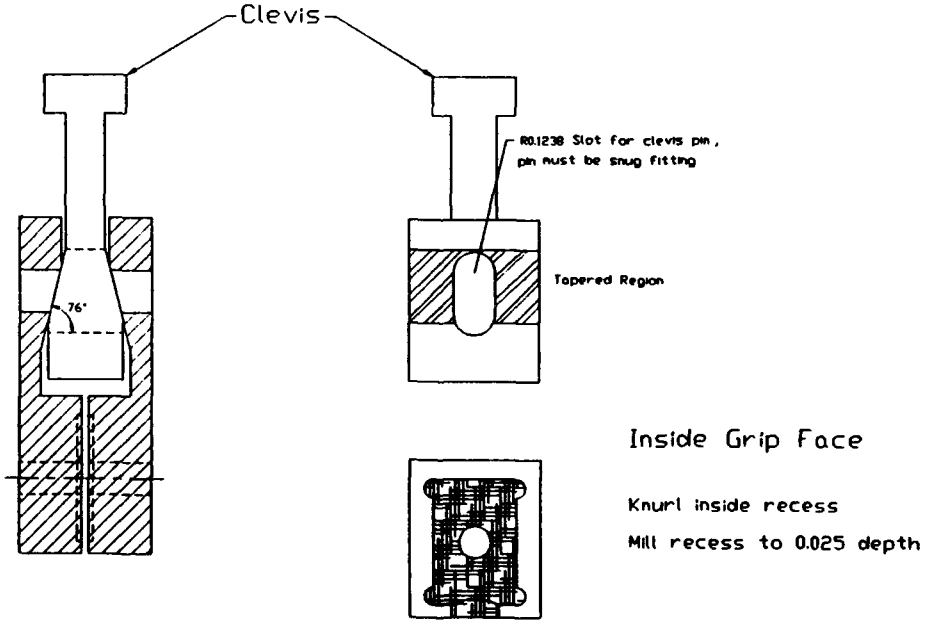

Figure 14. Self centering grip assembly used in creep test apparatus.

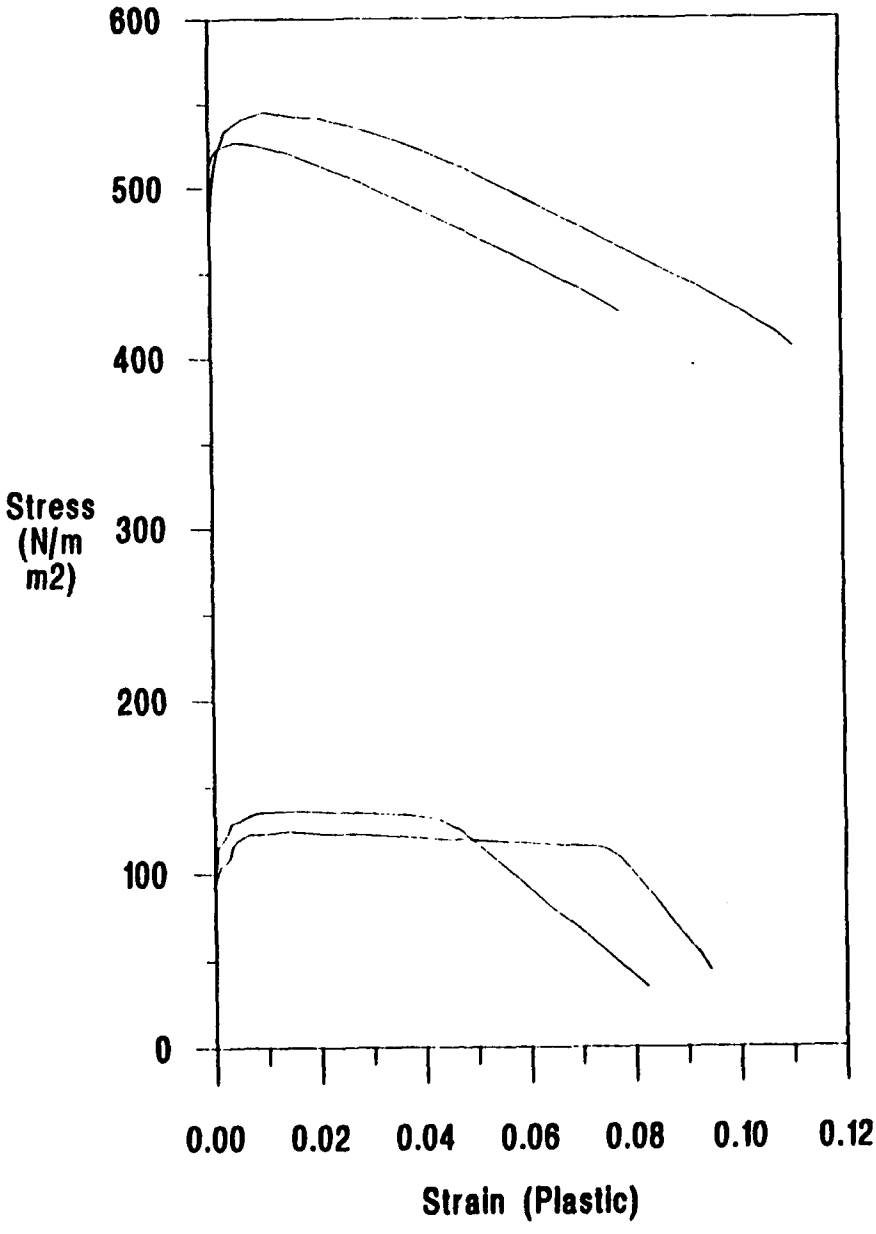

Figure 15. Stress vs plastic strain obtained at constant strain rates of 6.56×10^{-6} sec^{-1} and 6.56×10^{-5} sec^{-1} at room temperature and 400°C.

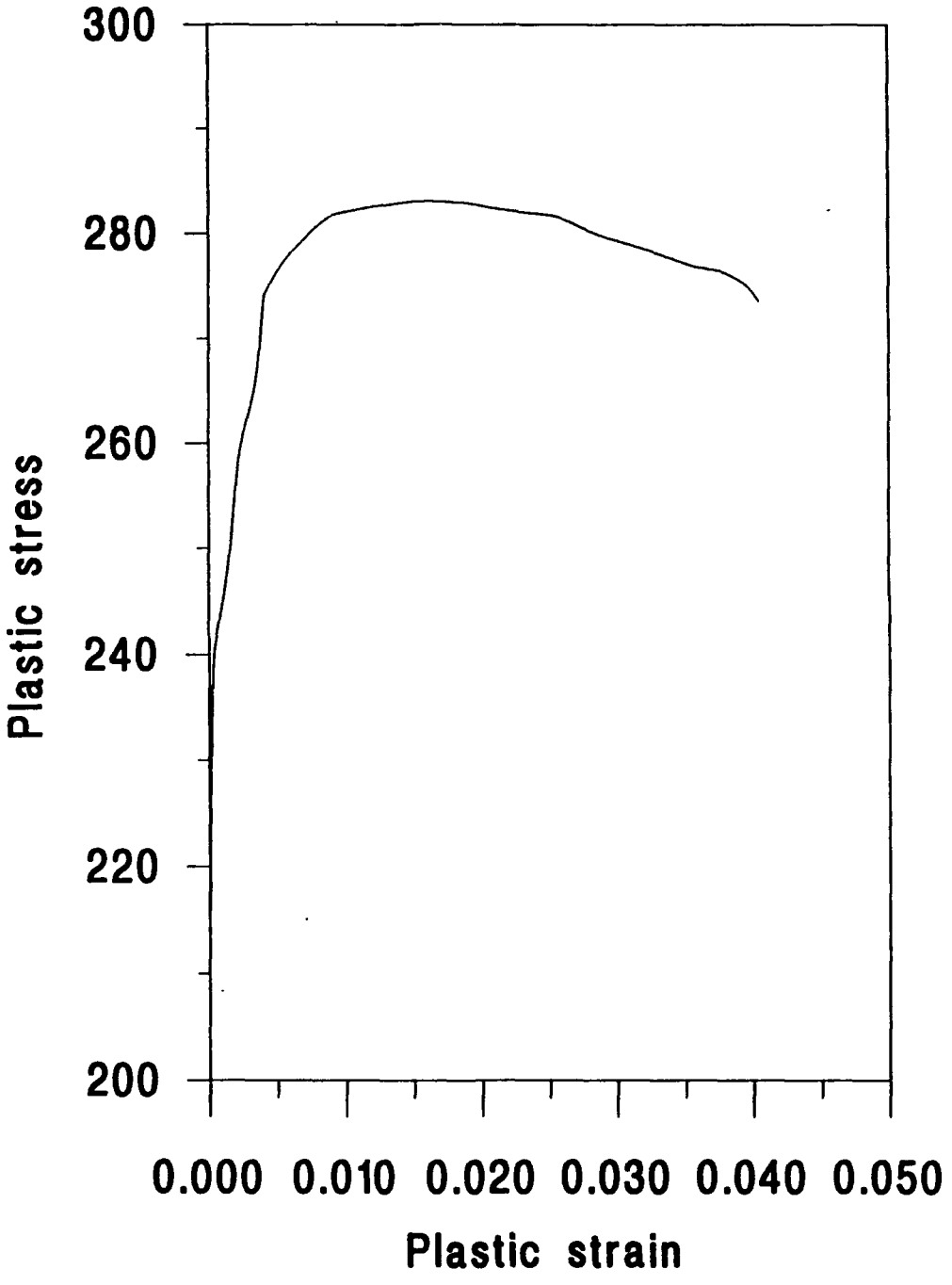

Figure 16. Stress vs plastic strain obtained at 6.56×10^{-5} sec^{-1} at 250°C.

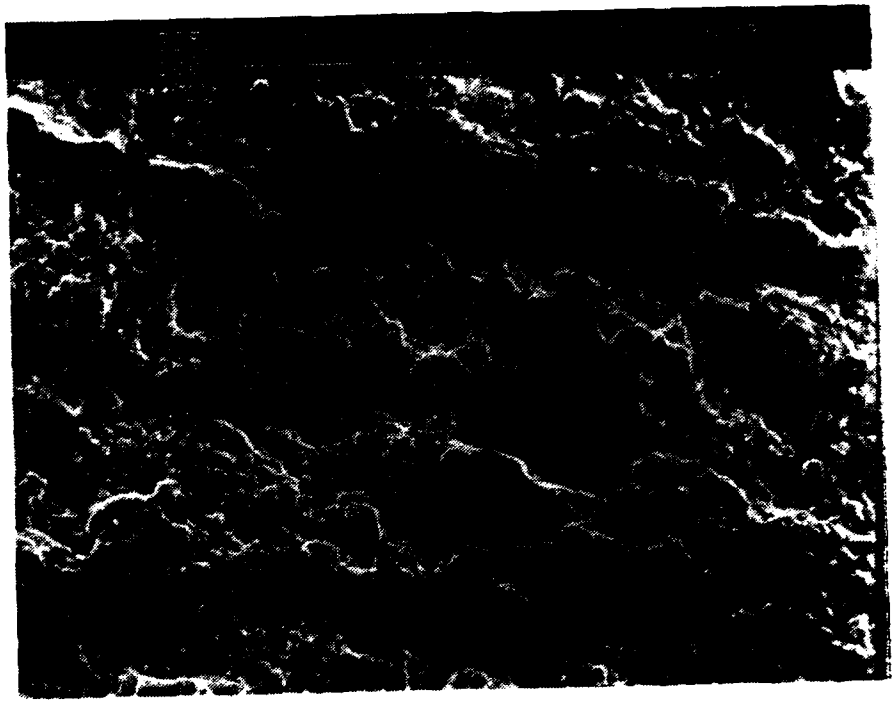

Figure 17. SEM micrograph of tensile fracture surface obtained at room temperature at 6.56 $x10^{-5}$ sec^{-1}.

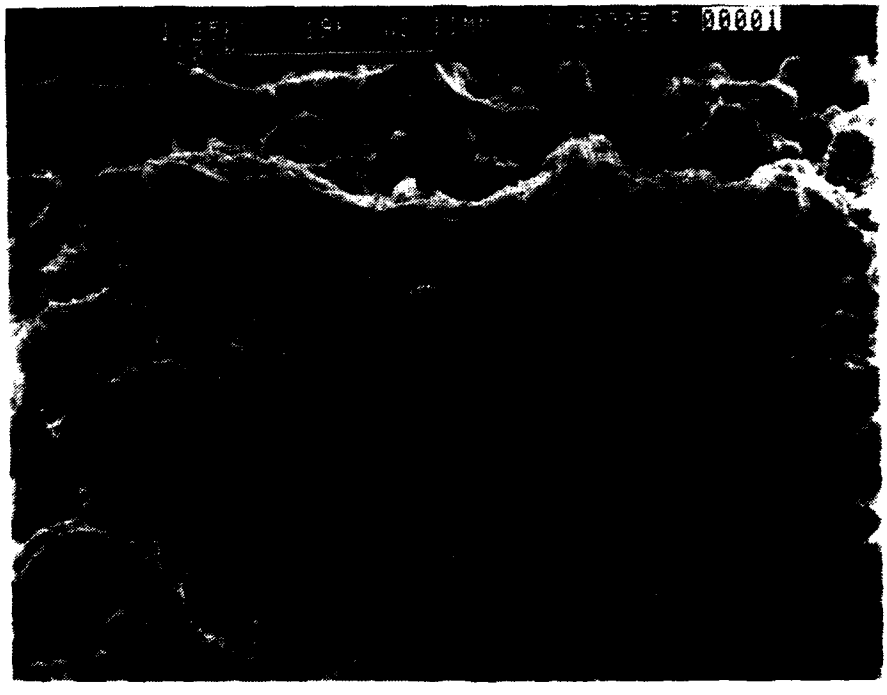

Figure 18. SEM micrograph of tensile fracture surface obtained at 400°C at 6.56 $x10^{-5}$ sec^{-1}.

Figure 19. SEM micrograph of tensile fracture surface obtained at 250 °C at 1.3 $x10^{-5}$ sec^{-1}.

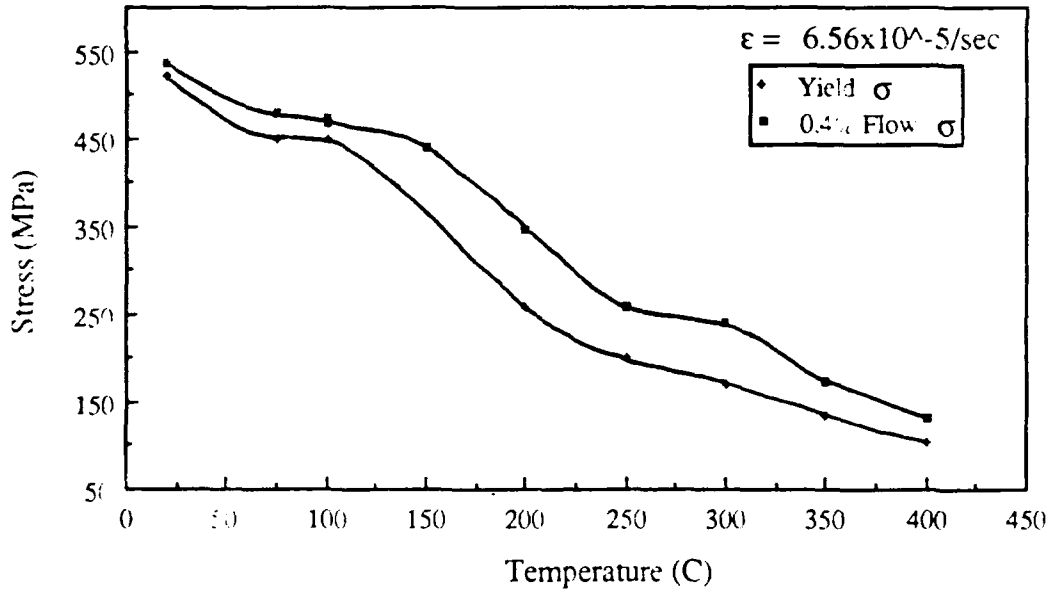

Figure 20. Yield and 0.4% flow stress vs temperature obtained at 6.56 $x10^{-5}$ sec^{-1}. Note plateau at 75° -100°C and 250° -300°C in 0.4% flow stress.

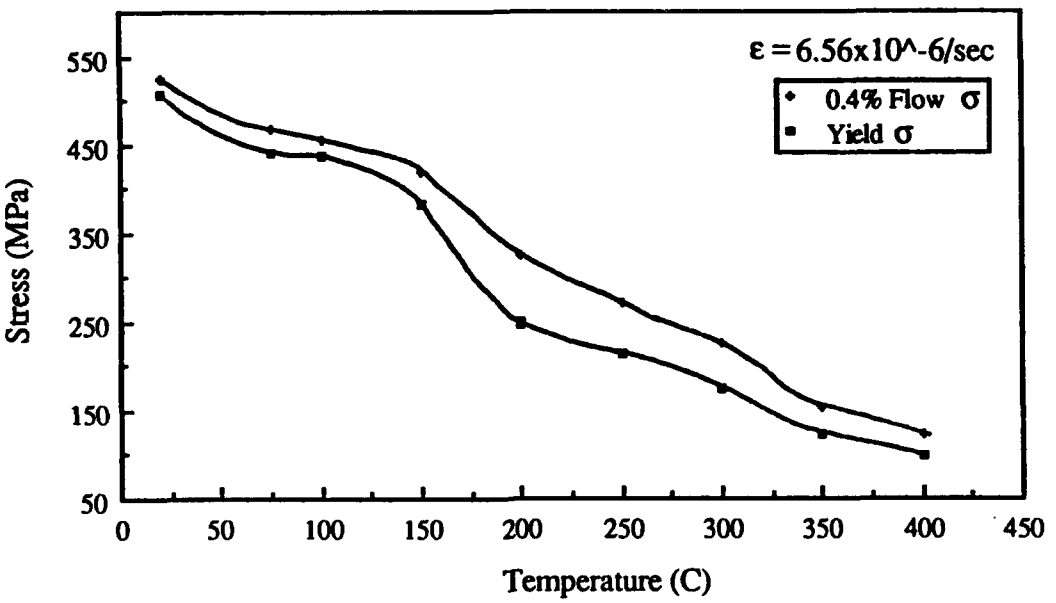

Figure 21. Yield stress and 0.4% flow stress vs temperature obtained at 6.56 x10^{-6} sec^{-1}. Note plateau centered at 75°C and 250°C.

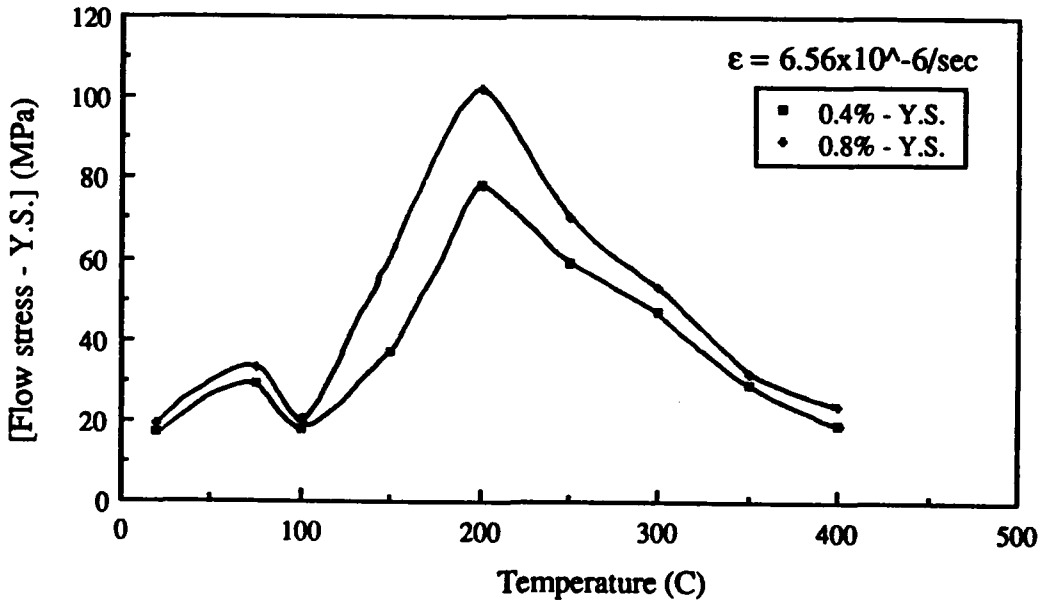

Figure 22. Flow stress -yield stress difference plotted vs temperature at 6.56 x10^{-6} sec^{-1}. Note large strain rate exhibited by large stress difference at 200°C.

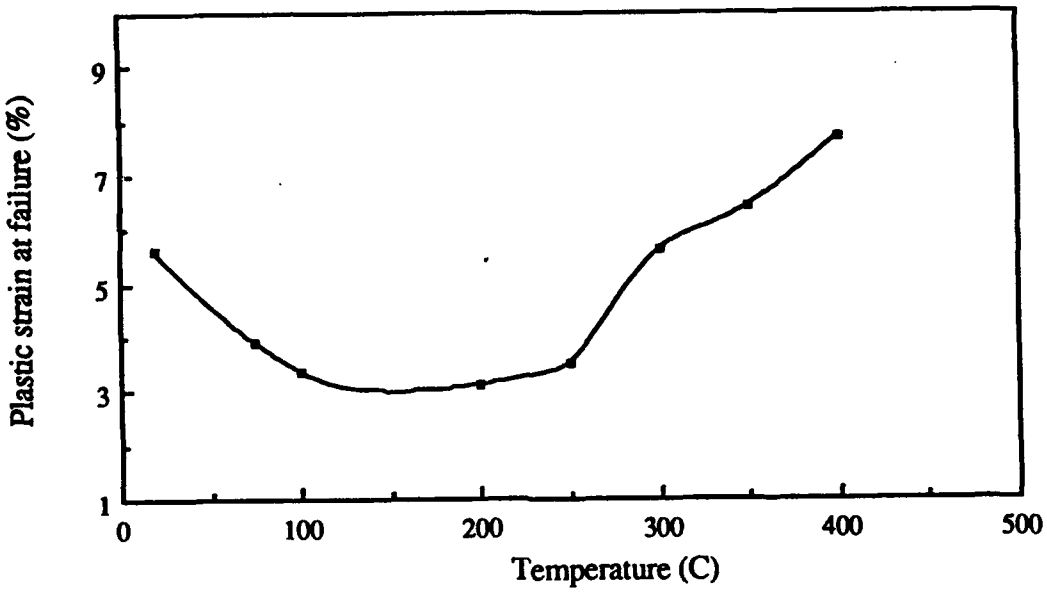

Figure 23. % elongation vs temperature obtained at 6.56 x10^{-6} sec^{-1}.

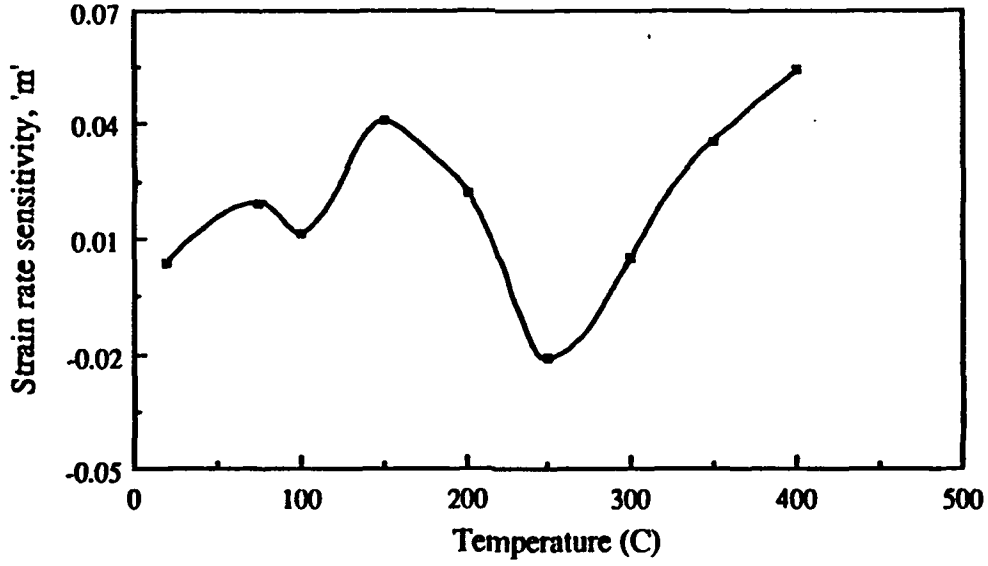

Figure 24. Strain rate sensitivity (m) vs temperature for FVS1212 using yield stress and strain rates of 6.56 x10^{-6} sec^{-1} and 6.56 x10^{-5} sec^{-1}.

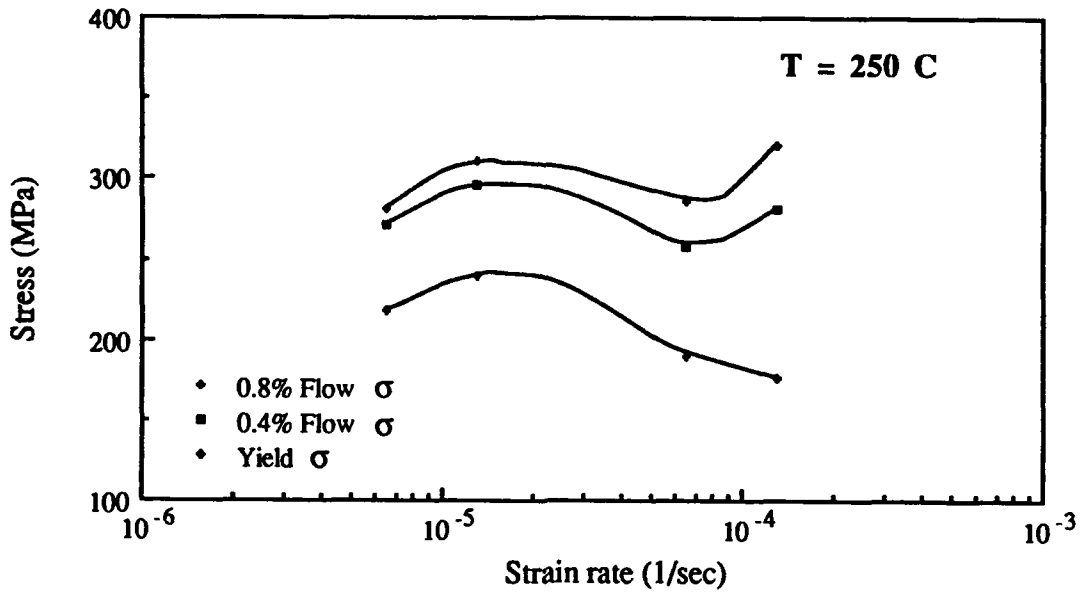

Figure 25. Flow stress vs strain rate at 250°C. Note large difference between yield stress and 0.4% and 0.8% flow stresses obtained at 1.3 $x10^{-4}$ sec^{-1}.

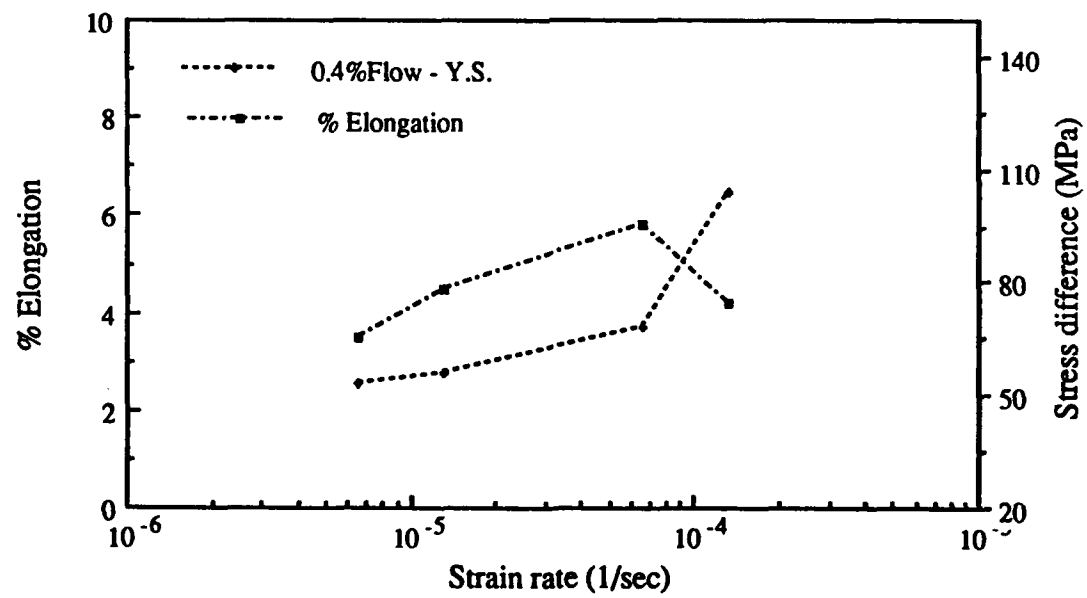

Figure 26. % elongation and flow stress difference vs strain rate at 250°C. Note drastic change at strain of 1.3 $x10^{-4}$ sec^{-1}.

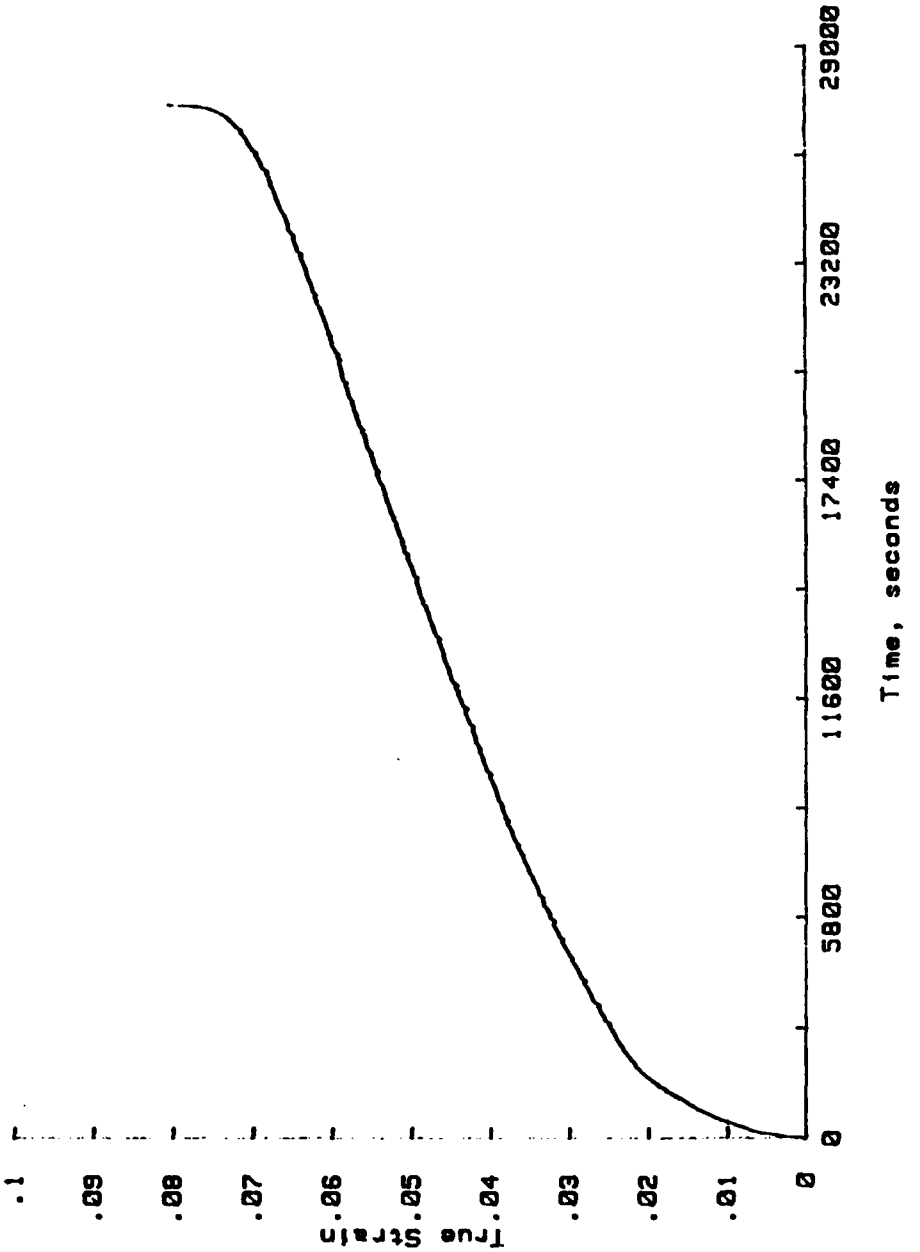

Figure 27. Typical strain vs time curve obtained from creep apparatus at 450°C and at 80MPa.

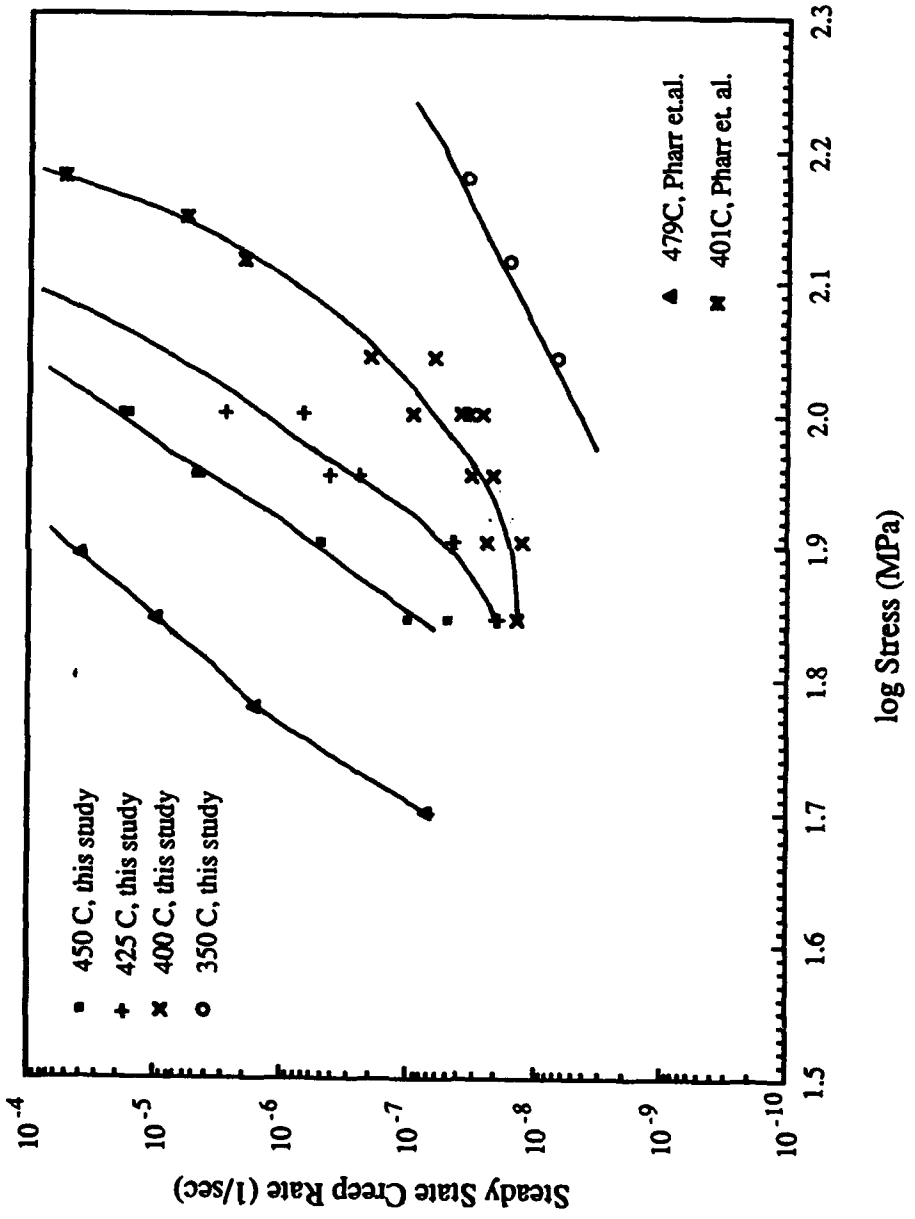

Figure 28. Steady state creep rate vs stress. Data from Pharr et al is also included [ref 15].

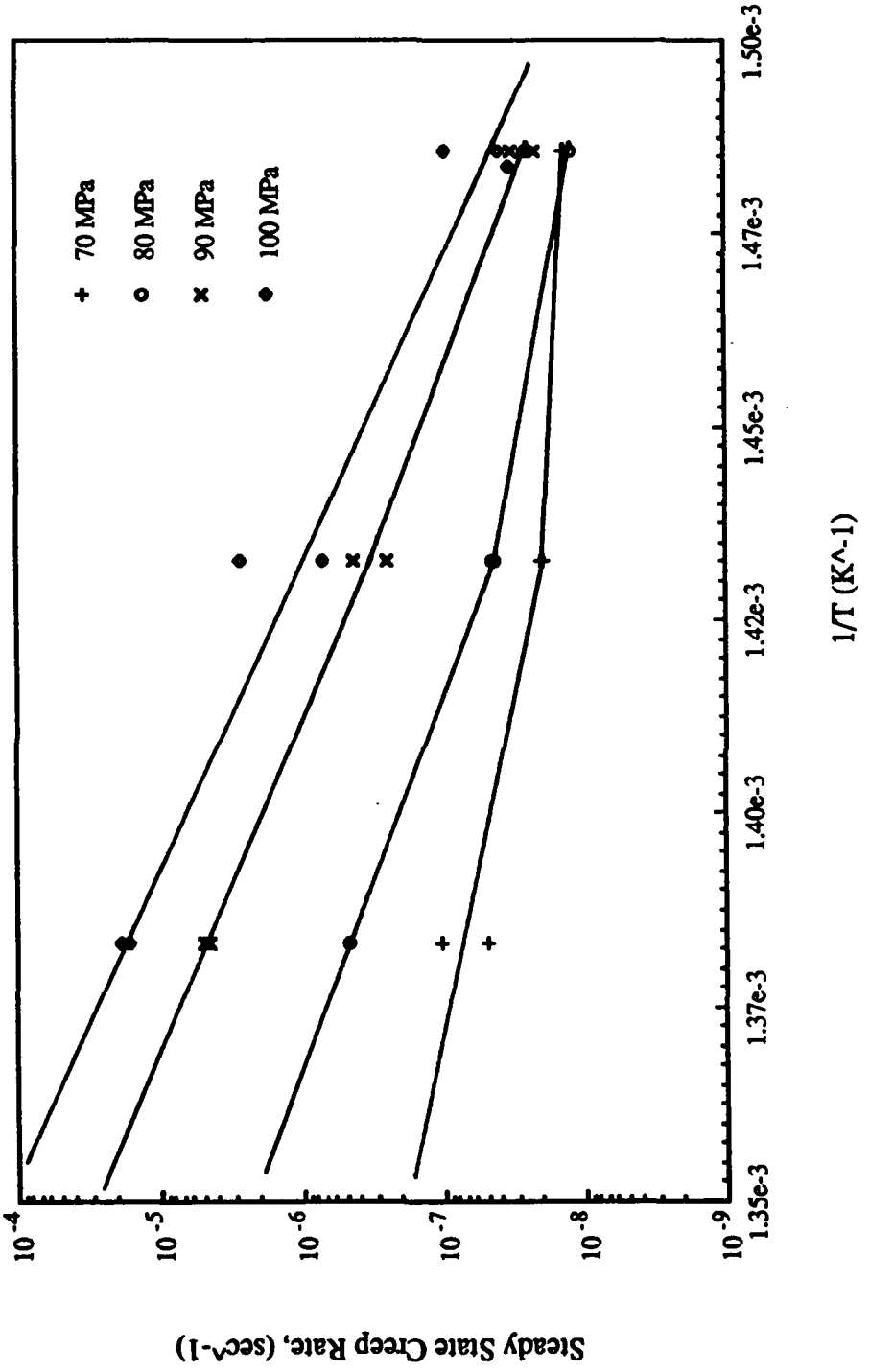

Figure 29. Steady state creep rate vs 1/temperature at various stress levels. Used for obtaining activation energies

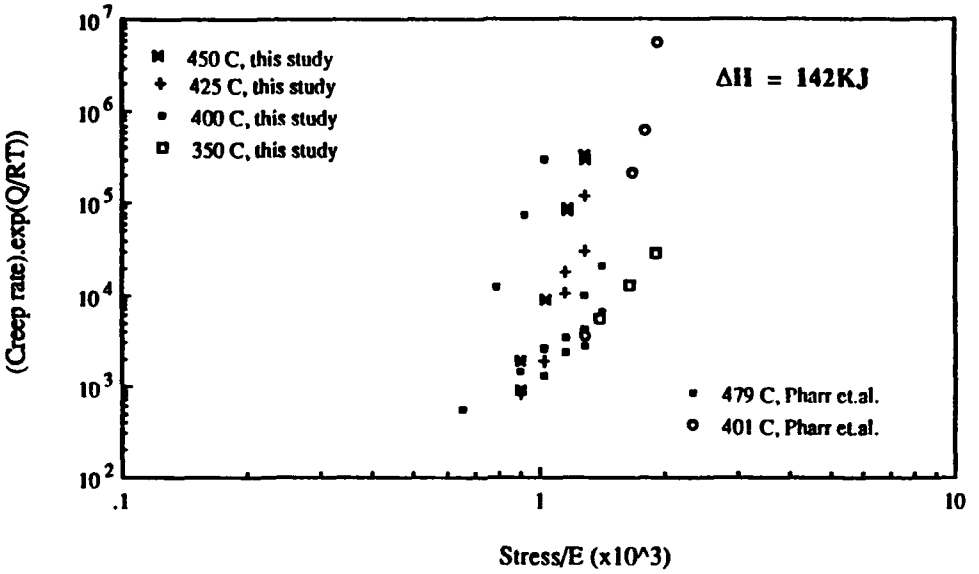

Figure 30. Temperature compensated strain rate vs modulus compensated stress using aluminum self-diffusion activation energy of 142 kJ/mole. Data obtained from Pharr et al is also included [ref 15].

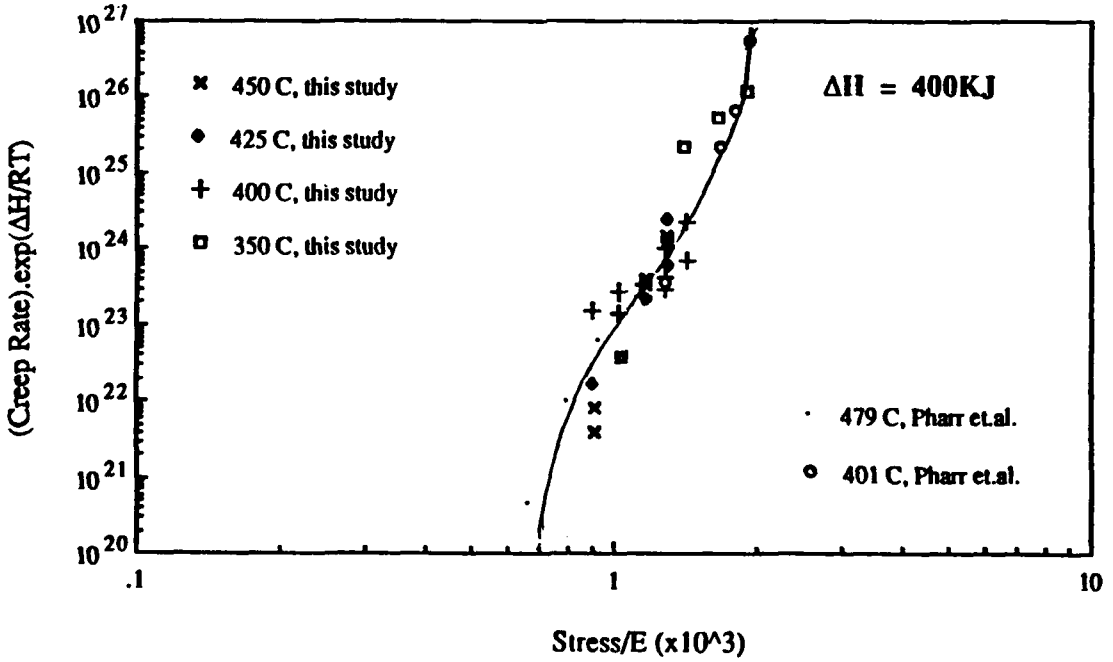

Figure 31. Temperature compensated strain rate vs modulus compensated stress using an activation energy of 400 kJ/mole. Data from Pharr et al is also included [ref 15].

LIST OF REFERENCES

1. Hildenman, G. J. and Koczak, M. J., "Aluminum Powder Alloys - An Overview", Advisory Group for Aerospace Research and Development Lecture Series, No. 174, pp. 5-1 - 5-25, 1990.

2. Skinner, D. J., Okazaki, K., and Adam, C. M., "Physical Metallurgy and Mechanical Properties of Aluminum Alloys Containing Eight to Twelve Weight Percent Iron", Rapidly Solidified Powder Aluminum Alloys, ASTM STP 890, M. E. Fine and E. A. Starke, Jr., Eds., American Society for Testing and Materials, pp. 211-236, 1986.

3. Raybould, D., "Forming of Rapidly Solidified Elevated Temperature Aluminum Alloys Produced by Planar Flow Casting", Dispersion Strengthened Aluminum Alloys, Y. W. Kim and W. M. Griffth, The Minerals, Metals, and Materials Society, pp. 199-215, 1988.

4. Cotton, J. D. and Kaufman, M. J., "Microstructural Evolution in Rapidly Solidified Al-Fe Alloys: An Alternative Explanation", Metallurgical Transaction A, Vol. 22A, pp. 927-934, 1991.

5. Skinner, D. J., "The Physical Metallurgy of Dispersion Strengthened Al-Fe-V-Si Alloys", Dispersion Strengthened Aluminum Alloys, edited by Y. W. Kim and W. M. Griffth, The Minerals, Metals, and Materials Society, pp 181-197, 1988.

6. Skinner, D. J., Rye, D., Raybould, D., and Brown, A. M., "Dispersion Strengthened Al-Fe-V-Si Alloys", Scripta Metallurgica, Vol. 20, pp. 867-872, 1986.

7. Rodriguez, M. A., and Skinner, D. J., "Compositional Analysis of the Cubic Silicide Intermetallic in Dispersion strengthened Al-Fe-V-Si Alloys", Journal of Material Science Letters, No. 9, pp. 1292-1293, 1990.

8. Franck, R. E., and Hawk, J. A., "Effect of Very High Temperatures on the Properties of Al-Fe-V-Si Alloy", Scripta Metallurgica, Vol. 23, No. 1, pp. 113-118, 1989.

9. Skinner, D. J., Zendalis, M. S., and Peltier, J., "Anomalous Ductility Variations at Intermediate Temperatures in Rapidly Solidified Al-base Alloys", light-Weight Alloys for Aerospace Applications, E. W. Lee, E. H. Chia, and N. J. Kim, The Minerals, Metals, and Material Society, pp 71-78, 1989.

10. Skinner, D. J., Zendalis, M. S., and Gilman, P., "Effect of Strain Rate on Tensile Ductility for a Series of Dispersion-strengthened Aluminum-based Alloys", Material Science and Engineering, A119, pp. 81-86, 1989.

11. Bouchaud, E., Kubin, L., and Octor, H., "Ductility and Dynamic Strain Aging in Rapidly Solidified Aluminum Alloys", Metallurgical Transactions A, Vol. 22A, pp. 1021-1028, 1991.

12. Evans, R. W., and Wilshire, B., Creep of Metals and Alloys, 1st ed., Dotesios Printers Ltd, 1985.

13. Edwards, G. R., McNelley, T. R., and Sherby, O. D., "Diffusion-Controlled Deformation of Particulate Composite", Phil. Mag., Vol. 32, pp. 1245- 1264, 1975.

14. Oliver, W. C., and Nix, W. D., "High Temperature Deformation of Oxide Dispersion Strengthened Al and Al-Mg Solid Solution", Acta Metallurgica, Vol. 30, pp. 1335-1347, 1982.

15. Pharr, G. M., Zedalis, M. S., Skinner, D. J., and Gilman, P. S., "High Temperature Creep Deformation of a Rapidly Solidified Al-Fe-V-Si Alloy", Dispersion Strengthened Aluminum Alloys, Y. W. Kim and W. M. Griffth, The Minerals, Metals, and Materials Society, pp. 309-322, 1988.

16. Benci, J. E., and Frazier, W. E., "Evaluation of a new Aluminum Alloy for 700 °F Aerospace Applications", Presentation, The Minerals, Metals, and Materials Society Conference, New Orleans, La., Feb. 1991.

17. Gilman, P. S., Zendalis, M. S., Peltier, J. M., and Das, S. K., "Rapidly Solidified Aluminum-Transition Metal Alloys for Aerospace Application", AIAA/AHS/ASEE Aircraft Design, Systems and Operations Conference, 1988.

18. Goodson, E. F., "The Stress and Temperature Dependence of Creep in an Al-2.0Wt%Li Alloy", Master's Thesis, Naval Postgraduate School, Monterey, California, 1989.

19. Coghlan, W. A., "Constant Stress Continuous Compression Creep Machine for Small Single Crystal", The review of Scientific Instruments, Vol. 43, pp. 464-467, 1972.

20. Freidel, J., Dislocations, pp. 24, Addision-Wesley, 1964.

21. Mondolfo, L. F., Aluminum Alloys: Structure and Properties, 2nd ed., pp. 24, Butterworth & Co. (Publishers) Ltd., 1979.

INITIAL DISTRIBUTION LIST

		No. Copies
1.	Defense Technical Information Center Cameron Station Alexandria, Virginia 22304-6145	2
2.	Library, Code 52 Naval Postgraduate School Monterey, California 93945-5002	2
3.	Weapons System Engineering Curricular Office Code 33 Naval Postgraduate School Monterey, California 93945	1
4.	Professor T. R. McNelley, Code ME/MC Department of Mechanical Engineering Naval Postgraduate School Monterey, California 93945	1
5.	Adjunct Professor S. Mitra, Code ME/MT Department of Mechanical Engineering Naval Postgraduate School Monterey, California 93945	1
6.	Lt. Matthew B. Cissel 110 West Tradewinds Rd WinterSprings, Florida 32708	1